© 2016. Published by The Company of Biologists Ltd | Development (2016) 143, 4452-4461 doi:10.1242/dev.129932

RESEARCH ARTICLE

Demethylation of ERECTA receptor genes by IBM1 histone demethylase affects stomatal development

Yuhua Wang[1], Xueyi Xue[2], Jian-Kang Zhu[1,3,*] and Juan Dong[2,4,*]

ABSTRACT

DNA methylation and histone modifications interact to modulate gene expression in biological organisms. The histone demethylase IBM1 suppresses DNA methylation and gene silencing, primarily by targeting genic regions in the *Arabidopsis* genome. The chromatin regulator EDM2 is also required for prevention of genic DNA methylation because it maintains *IBM1* expression by promoting *IBM1* mRNA distal polyadenylation. Loss-of-function *ibm1* and *edm2* mutant plants display a wide range of developmental defects, but little is known about which developmentally important genes are regulated by IBM1 and EDM2. Here, we show that both *ibm1* and *edm2* mutants display defects in production of stomatal lineage cells, which is linked to DNA hypermethylation of the ERECTA family genes, including *ER*, *ERL1* and *ERL2*. Stomatal phenotypes and DNA methylation levels of ER genes in *ibm1* and *edm2* mutants are restored by mutations in the genes encoding the histone methyltransferase KYP and DNA methyltransferase CMT3. Our data demonstrate that a specific plant developmental context is influenced by IBM1-regulated histone modification and DNA methylation on the gene body region of the ERECTA receptors.

KEY WORDS: ER receptors, DNA methylation, Stomatal development, IBM1 histone demethylase, EDM2 chromatin regulator

INTRODUCTION

DNA cytosine methylation and histone modification closely interact to silence gene expression (Fuks, 2005). Histone 3 lysine 9 (H3K9) dimethylation is associated with heterochromatin formation, DNA hypermethylation and thereby gene silencing in both plants and mammals (Badeaux and Shi, 2013; Liu et al., 2010). *INCREASE IN BOSAI METHYLATION 1* (*IBM1*) encodes a histone demethylase that contains a JmjC-domain and belongs to the JHDM2/KDM3 family (Klose et al., 2006; Saze et al., 2008). Mutations in *IBM1* not only result in increased H3K9 dimethylation, but also cause ectopic DNA methylation, mainly in gene bodies but not transposons (Inagaki et al., 2010; Miura et al., 2009). Recently, the putative chromatin regulator ENHANCED DOWNY MILDEW 2 (EDM2) was found to function upstream of IBM1 to maintain the expression of functional IBM1 by promoting the distal polyadenylation of its transcripts (Lei et al., 2014). Consistent with this direct genetic interaction between *IBM1* and *EDM2*, almost 90% of hypermethylated loci in *edm2* mutant plants overlapped with those in the *ibm1* mutant (Lei et al., 2014). As a consequence of the extensive DNA hypermethylation in gene bodies, both *edm2* and *ibm1* mutations affect plant development in many aspects. The *edm2* and *ibm1* mutants show abnormally curved leaves, arrested flowers, reduced fertility and aborted seed development (Saze et al., 2008). EDM2 also promotes floral transition by acting upstream of FLOWERING LOCUS C (FLC) (Tsuchiya and Eulgem, 2010a) and facilitates the growth features related to vegetative phase change in *Arabidopsis* (Tsuchiya and Eulgem, 2010b). Thus far, little progress has been made towards understanding the specific downstream genes regulated by IBM1 and EDM2 in plant developmental programs.

The RNA-directed DNA methylation (RdDM) pathway is required for *de novo* DNA methylation and maintenance of methylation in the CHH (where H is A, T or C) sequence context (Matzke et al., 2015; Zhang and Zhu, 2011; Law and Jacobsen, 2010). RdDM requires tightly coordinated activities of DOMAINS REARRANGED METHYLTRANSFERASE 2 (DRM2), RNA POLYMERASE II-RELATED RNA POLYMERASE IV and V (Pol IV and V) (Wierzbicki et al., 2008; Zheng et al., 2009), RNA-DEPENDENT RNA POLYMERASE 2 (RDR2), DICER-LIKE 3 (DCL3), ARGONAUTE 4 and 6 (AGO4/6), and many other proteins (Matzke et al., 2015). Maintenance of CG and CHG methylation requires MET1 and CMT3, respectively (He et al., 2011; Law and Jacobsen, 2010). DNA methylation by the plant-specific DNA methyltransferase CMT3 (Bartee et al., 2001; Lindroth et al., 2001) is guided by dimethylation of histone H3 at lysine 9 (H3K9me2) (Malagnac et al., 2002), which is catalyzed by the histone methyltransferase KRYPTONITE (KYP; also known as SUVH4) (Jackson et al., 2002; Ebbs et al., 2005). Mutations in the histone H3K9me2 demethylase IBM1 cause widespread gene body CHG methylation and developmental defects in *Arabidopsis* (Saze et al., 2008). The defects of *ibm1* mutants are fully suppressed by *cmt3* and *kyp* mutations, but not by mutations in the RdDM machinery (Miura et al., 2009; Saze et al., 2008).

Stomata are microscopic pores in the epidermis of leaves, stems and many other aerial organs in plants that control gas exchange between plants and the atmosphere. The production and patterning of stomata are controlled by a relatively linear signaling pathway (reviewed by Lau and Bergmann, 2012; Pillitteri and Dong, 2013; Pillitteri and Torii, 2012), which is initiated by extracellular peptide ligands in the EPIDERMAL PATTERNING FACTOR (EPF) family (Rowe and Bergmann, 2010; Torii, 2012); this signal is perceived by a receptor-like protein, TOO MANY MOUTHS (TMM) (Nadeau and Sack, 2002), and the LEUCINE-RICH REPEAT (LRR) receptor-like kinase family, including ERECTA (ER), ER-LIKE 1 (ERL1) and ER-LIKE 2 (ERL2) (Shpak et al., 2005). The ligand-receptor signaling is then delivered by a canonical MAP kinase cascade to modulate cytoplasmic and

[1]Shanghai Center for Plant Stress Biology, Shanghai Institute for Biological Sciences, Chinese Academy of Sciences, Shanghai 200032, China. [2]Waksman Institute of Microbiology, Rutgers, The State University of New Jersey, Piscataway, NJ 08854, USA. [3]Department of Horticulture and Landscape Architecture, Purdue University, West Lafayette, IN 47906, USA. [4]Department of Plant Biology and Pathology, Rutgers, the State University of New Jersey, New Brunswick, NJ 08901, USA.

*Author for correspondence (dong@waksman.rutgers.edu; jkzhu@sibs.ac.cn)

J.D., 0000-0002-3089-3167

Received 17 August 2015; Accepted 19 September 2016

Development (2016) 143, 4452-4461 doi:10.1242/dev.129932

nuclear machineries in stomatal production and division patterning. Mutations in these signaling components, including the EPF peptides and ER receptors, lead to mis-patterned stomatal distribution and overproliferation of the stomatal lineage cells (Hara et al., 2007, 2009; Hunt and Gray, 2009; Shpak, 2013; Torii, 2012).

To investigate how epigenetic modifications, e.g. histone H3K9 methylation and DNA methylation, might affect plant development, we examined the loss-of-function *Arabidopsis* mutants *ibm1* and *edm2*. We found that these mutants bear an increased number of stomatal lineage cells in the leaf epidermis. We show that the stomatal defects in *edm2* mutants are caused by the impaired expression of *IBM1*. We further elucidated that three ER genes (*ER*, *ERL1* and *ERL2*), but not other stomatal genes, are hypermethylated in the absence of *IBM1* or *EDM2*, which in turn results in lowered transcript level and thus abnormal stomatal patterning. The ER receptors belong to the large gene family of LRR receptor-like kinases and play important roles in cell division, proliferation and differentiation in various plant developmental processes (Shpak, 2013; van Zanten et al., 2009). Our results therefore provide new insights into the ER gene family as an integration point where the chromatin regulators IBM1 and EDM2 modulate plant development at an epigenetic level.

RESULTS

Stomatal lineage divisions are overproduced in *ibm1* and *edm2* mutants

The loss-of-function mutants of *ibm1* and *edm2* show a variety of developmental defects in *Arabidopsis* leaves, flowers and seeds (Eulgem et al., 2007; Saze et al., 2008; Tsuchiya and Eulgem, 2010a,b). Here, we examined stomatal development and patterning defects. The lines under analysis are three independent alleles, *ibm1-1*, *ibm1-3* and *ibm1-4* (Lei et al., 2014; Fan et al., 2012), and two alleles of *edm2-4* and *edm2-5* (Lei et al., 2014). We found that all of these mutants produce more cell divisions, probably within the stomatal lineage, in the 3-dpg (days post-germination) adaxial cotyledons (Fig. 1A-F). The number of small dividing cells in *ibm1* and *edm2* mutants was about twice that of the Columbia (Col) wild-type plants (Fig. 1G,H) and the elevated stomatal lineage divisions persist in older leaves (16-dpg cotyledons and 12-dpg true leaves) of *ibm1* and *er* mutants, but not in Col (Figs S1, S2).

To identify visually the small dividing cells in *ibm1* and *edm2*, we crossed two marker lines, MUTEp-nucGFP (nuclear GFP driven by the *MUTE* promoter) and TMMp-GFP (GFP driven by the *TMM* promoter), into the *ibm1-1* mutant. The expression of MUTEp-nucGFP marks the meristemoids that are differentiating into guard mother cells (Pillitteri et al., 2007) and TMMp-GFP labels the stomatal lineage cells (Nadeau and Sack, 2002). As expected, the small dividing cells in *ibm1*-1 are positive for both markers (Fig. 2A-D) and the numbers are greatly increased compared with the wild type (Col) (Fig. 2E).

Stomatal defects in *edm2* can be rescued by ectopic expression of the *IBM1-Long* transcripts

The putative chromatin regulator EDM2 functions to regulate the expression of *IBM1* (Lei et al., 2014). To investigate the genetic interaction between *ibm1* and *edm2* in stomatal development, we generated a double mutant of *ibm1-1 edm2-4* and found that the

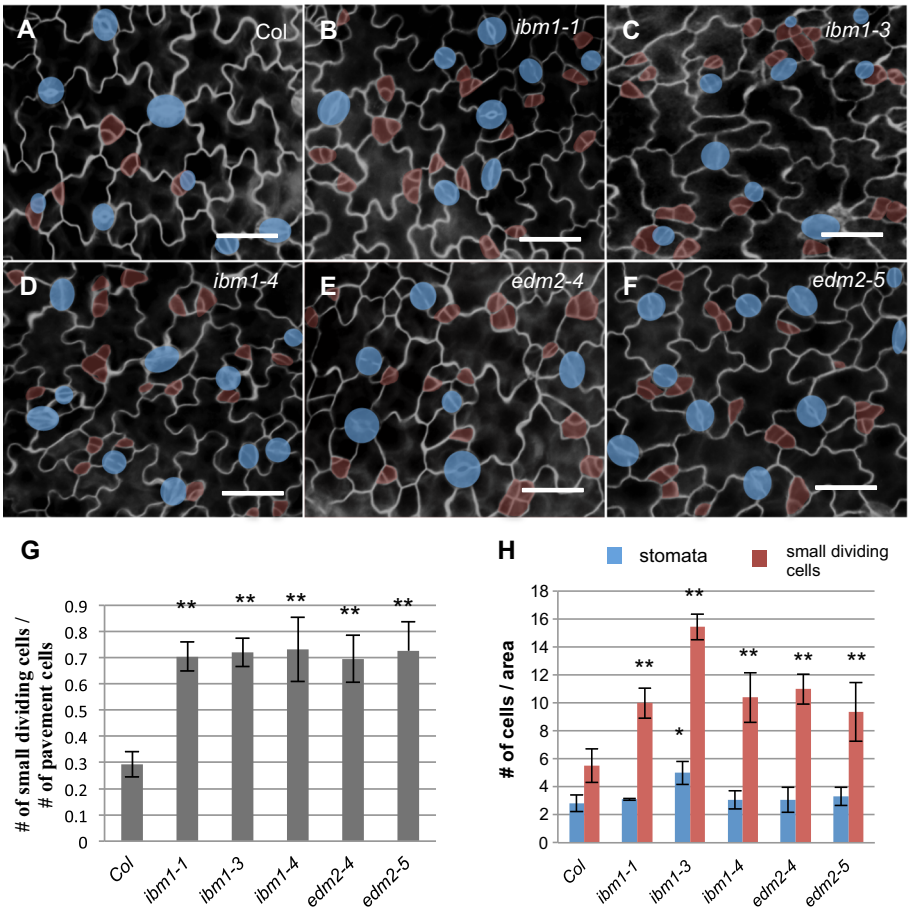

Fig. 1. *ibm1* and *edm2* mutants generate more stomatal divisions in the leaf epidermis. (A-F) Epi-fluorescence images of 3-dpg adaxial cotyledons of wild type (Col; A), *ibm1-1* (B), *ibm1-3* (C), *ibm1-4* (D), *edm2-4* (E) and *edm2-5* (F). The images in A and D are also shown in Fig. 4D and Fig. 4F, respectively, because these experiments were performed concurrently. Stomata are shaded blue; small dividing cells are highlighted in red. Remarkably elevated numbers of small dividing cells were evident in *ibm1* and *edm2* mutants. Cell outlines were stained with FM1-43. Scale bars: 20 µm. (G) Histogram showing the ratio of total number of small dividing cells relative to that of pavement cells in different genotypes. (H) Quantification of stomata and small dividing cells in the indicated plants. For each sample, cells were counted from similarly positioned areas of 122,500 µm^2 in 3-dpg cotyledons. In G and H, data are mean±s.d., n=6 individual cotyledons for each line. This quantification method applies to all other figures that demonstrate stomatal phenotype in this study. *P<0.05, **P<0.01; Student's t-test with Bonferroni correction was used to compare the mutant values with those of Col.

Development (2016) 143, 4452-4461 doi:10.1242/dev.129932

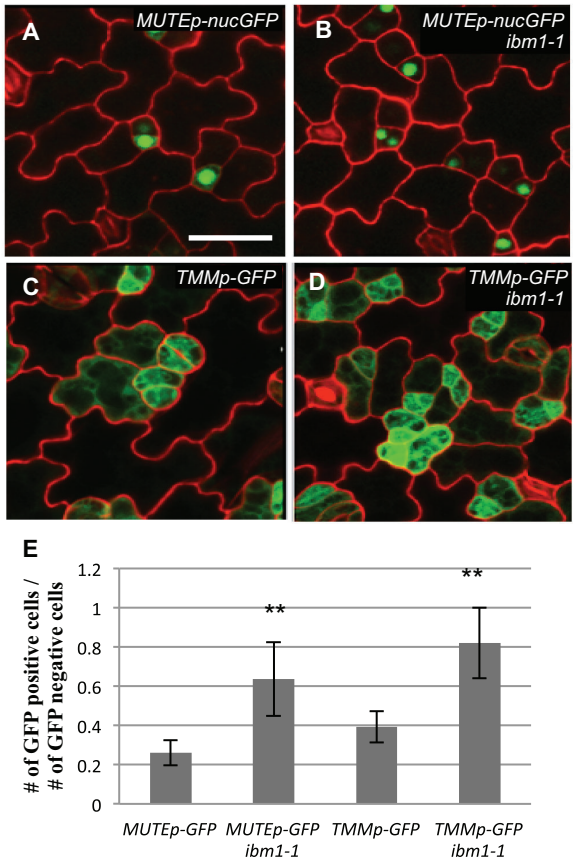

Fig. 2. Overproduction of stomatal lineage cells in *ibm1* mutants. (A-D) Confocal images of 3-dpg adaxial cotyledons expressing cell identity markers (green). Cell outlines are stained with FM4-64 (red). Scale bar: 30 µm (in A, for A-D). (A,B) The meristemoid marker MUTEp-nucGFP (nuclear GFP) in Col (A) and *ibm1-1*(B). (C,D) The stomatal lineage marker TMMp-GFP in Col (C) and *ibm1-1* (D). More cells expressing GFP were evident in *ibm1-1* mutants. (E) Histogram showing the ratio of the number of GFP-positive cells over that of GFP negative. **P*<0.05, ***P*<0.01; Student's *t*-test with Bonferroni correction (*n*=6; ±s.d.) was used to compare the marker lines in *ibm1-1* with the wild type.

stomatal phenotype of the double mutant resembled that of the single mutants of *ibm1*-1 or *edm2-4* (Fig. 3A,B,F,G). Because *ibm1-1 edm2-4* appeared to grow smaller leaves, the number of cells per area in the double mutant appeared to be relatively high (Fig. 3G), but the ratio of stomatal lineage cells versus pavement cells (more reflective of stomatal development) was comparable to that of the single mutants (Fig. 3F). These data suggested that *EDM2* and *IBM1* do indeed function in the same genetic pathway for proper stomatal production.

The detectable transcripts of *IBM1* contain at least two variants (short and long) and EDM2 is required for the accumulation of the long version (*IBM1-L*) (Lei et al., 2014). EDM2 binds to the intronic heterochomatin region of *IBM1* gene, and blocks the proximal polyadenylation that produces *IBM1-S* to promote distal polyadenylation, which produces *IBM1-L* (Lei et al., 2014). Previous work showed that when the intronic heterochromatin region of *IBM1* was deleted, the accumulation of *IBM1-L* no longer required *EDM2* (Lei et al., 2014). Here, we found that, indeed, when driven by the endogenous promoter, the genomic region of the *IBM1* gene with a 764-bp deletion of the intronic heterochromatin fragment (*gIBM1-ΔIH*), which produces functional *IBM1-L* (Lei et al., 2014), largely rescued the stomatal defects of *edm2* (Fig. 3C,D,F-G). By contrast, the wild-type version of *IBM1* (*gIBM1*) failed to rescue the defects of *edm2-4* in stomatal development (Fig. 3C). As a control, the genomic *EDM2* fragment rescued the stomatal phenotype in *edm2* mutants (Fig. 3E-G). Taken together, these data suggested that the elevated number of stomatal asymmetric cell divisions in *edm2* mutants is caused by deficient expression of functional *IBM1-L* transcripts.

Hypermethylation and silencing of the ER family genes in *ibm1* and *edm2*

It was reported that IBM1, as a histone demethylase, functions to prevent gene body methylation and that *ibm1* loss-of-function mutants bear ectopic H3K9me2 and CHG hypermethylation in the gene body of thousands of active genes (Inagaki et al., 2010). The leaf epidermal patterning in *ibm1* and *edm2* to a certain extent phenocopied that of the loss-of-function mutants of the negative regulators in the signaling pathway during stomatal development, e.g. *erecta* (*er105*) (Shpak et al., 2004), *tmm* (Nadeau and Sack, 2002), *epf1* (Hara et al., 2007) and *epf2* (Hara et al., 2009; Hunt and Gray, 2009), though they did not show major defects in stomatal patterning (clusters) as was observed in *epf1* and *tmm* mutants. We scanned the whole-genome bisulfite sequencing database (Lei et al., 2014) and examined the DNA methylation levels of the stomatal development-related genes in different genetic backgrounds (Fig. 4A-C; Table S1). Among them, the coding regions of *ER*, *ERL1* and *ERL2* contain moderately methylated cytosine sites in Col (Fig. 4A-C). Interestingly, in *ibm1-4* and *edm2-4* mutants, the DNA methylation levels in *ER*, *ERL1* and *ERL2* were dramatically elevated (>25 fold) compared with those in the wild type (Col) (Fig. 4A-C; Table S1).

By contrast, most of the other stomata-related genes that we examined did not show an obvious increase (fold change <2) in methylation level in *ibm1* and *edm2* mutants (Table S1, a few exceptions showed two- to tenfold change). These genes include those encoding the transcription factors SPCH (MacAlister et al., 2007), MUTE (Pillitteri et al., 2007), FAMA (Ohashi-Ito and Bergmann, 2006), FOUR LIPS (Lai et al., 2005) and SCREAM (Kanaoka et al., 2008), and those encoding the signaling molecules TMM (Nadeau and Sack, 2002), EPF1 (Hara et al., 2007) and EPF2 (Hara et al., 2009; Hunt and Gray, 2009), as well as STOMAGEN (Kondo et al., 2010; Sugano et al., 2010), MKK7 and 9 (Lampard et al., 2009), MPK3 and 6 (Wang et al., 2007). *MYB88* is an exception that showed CHG elevation in *ibm1* mutants, but loss of *MYB88* alone does not produce a discernable stomatal phenotype (Lai et al., 2005). Interestingly, a CHG methylation reduction was found in *SPCH* (Table S1), though the transcription level of *SPCH* was not obviously affected (Fig. 5E), therefore the possible connection to *ibm1* stomatal overproduction cannot be assumed.

The stomatal defects in *ibm1* and *edm2* mutants to a certain extent resembled those of the *ERECTA* loss-of-function mutant *er105* (Shpak et al., 2005) (Fig. 4D-G), in that the stomatal entry divisions were considerably increased (red shades in Fig. 4E,F vs 4D; quantification in Fig. 4H,I) and the total numbers of stomata were mildly elevated (Fig. 4I). We crossed *ibm1* mutants to *er105* and found that the double mutants *ibm1-4 er105* (Fig. 4G) and *ibm1-1 er105* (Fig. S3A,B) both showed a similar level of stomatal phenotype to that of *er105* (Fig. 4H,I). At the whole-plant level, 3-week-old plants of *ibm1-1 er105* mainly bear morphological features of *er105* (Fig. S3B). These data strongly suggested that *er* is epistatic to *ibm1* in stomatal and early leaf development. To improve our understanding of the DNA methylation change in the three sequence contexts (CG, CHG and CHH) in *ibm1*, we performed

Development (2016) 143, 4452-4461 doi:10.1242/dev.129932

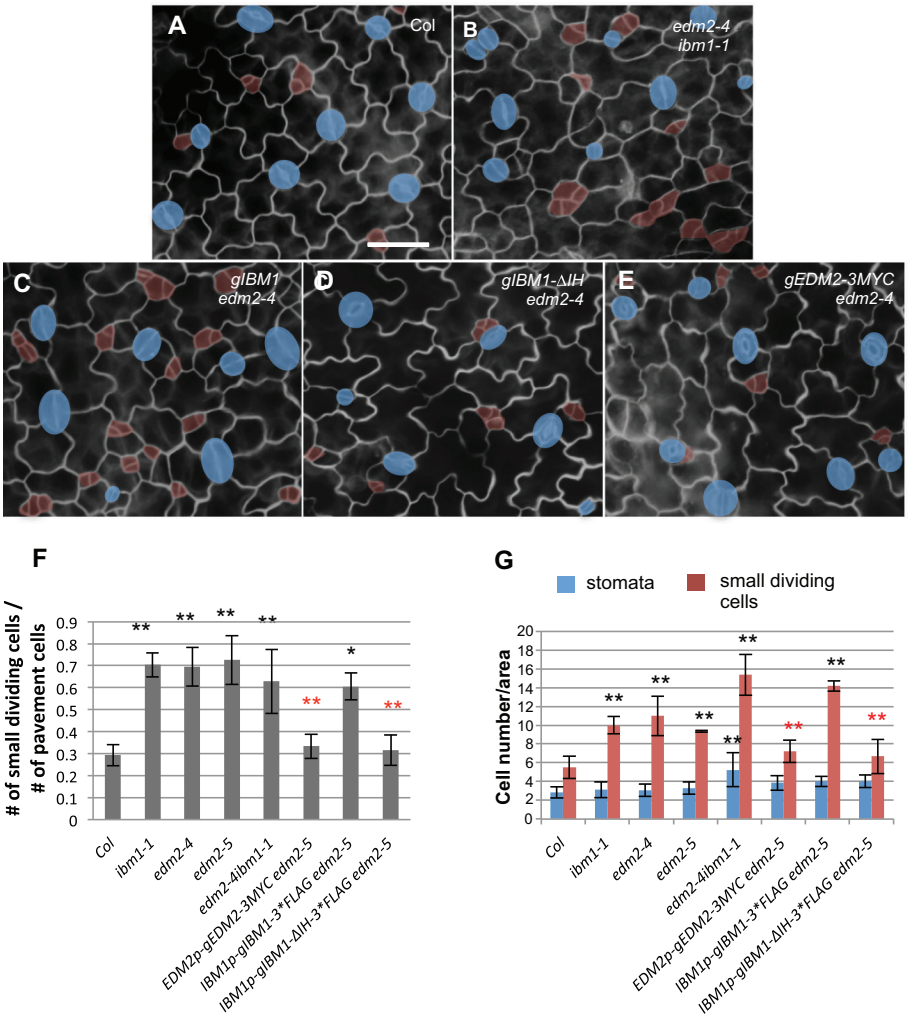

Fig. 3. Stomata defects in *edm2* are caused by impaired expression of *IBM1*. (A-E) Epi-fluorescence images of 3-dpg adaxial cotyledons of Col (A), *edm2-4 ibm1-1* (B), IBM1-gDNA in *edm2-4* (C; full-length genomic *IBM1*), gIBM1-ΔIH in *edm2-4* (D; the intron region deleted from *gIBM1*) and EDM2-gDNA-3*Myc in *edm2-4* (E; full-length genomic *EDM2*). The control image (A) is also shown in Fig. 6A because these experiments were performed concurrently. The double mutant *edm2-4 ibm1-1* produced more stomatal lineage cells. The full-length *IBM1* failed to rescue *edm2*, but the intron-minus version did. Blue shades indicate stomata, and small dividing cells are highlighted by red. Scale bar: 30 µm (in A, for A-E). (F) Histogram showing the ratio of the total number of small dividing cells relative to that of the pavement cells in different genotypes. The double mutant *edm2-4 ibm1-1* resembles the single mutants of *ibm1-1* and *edm2-4*. Successful complementation was found by *EDM2* transgene, as well as truncated *IBM1* transgene (*ΔIH*), but not by the full-length *IBM1*. **P*<0.05, ***P*<0.01; Student's *t*-test with Bonferroni correction. Black asterisks indicate significantly different from Col and red asterisks indicate significantly different from *edm2*-5.
(G) Quantification of the total number of stomata and small dividing cells in the indicated mutants. The same format of statistical analysis is used as in F.

bisulfite sequencing on individual loci of *ER*, *ERL1* and *ERL2* genes in Col, *ibm1-1* and *ibm1-4* mutants, respectively. The genomic regions examined by bisulfite sequencing are underlined in Fig. 4A-C. Consistent with the whole-genome methylation data, the individual locus methylation data confirmed that the gene bodies of *ER*, *ERL1* and *ERL2* are hypermethylated in both *ibm1-1* and *ibm1-4* mutants (Fig. 5A-C). It is also evident that the three tested ER genes showed the most dramatic elevation in CHG methylation, compared with CG and CHH methylation, when *IBM1* was disrupted (Fig. 5A-C). The promoter regions of the ER family genes were not obviously subjected to DNA methylation regulation in Col, *ibm1* and *edm2* plants (Fig. S4).

To correlate DNA methylation with gene expression level, we then analyzed transcription level of the ER genes. Real-time PCR experiments using 3-dpg seedlings showed that, in line with the elevated DNA methylation levels, expression levels of the ER genes were reduced by about 40% in *ibm1* and *edm2* mutants (Fig. 5D). By contrast, the expression levels of other stomatal regulatory genes mentioned above, including positive regulators (*SPCH* and *FAMA*) and negative regulators (*EPF1*, *EPF2* and *TMM*), were not consistently increased in the two alleles of *ibm1* mutants (Fig. 5E). The expression of *MUTE* was slightly enhanced (Fig. 5E), probably owing to overproduced stomatal lineage cells in *ibm1*. These data suggest that the stomatal defects in *ibm1* and *edm2* mutants are mainly caused by the decreased expression of three ER genes.

We further analyzed other receptor-like kinases that are phylogenetically related to the ER receptor family (Shiu and Bleecker, 2001): the brassinosteroid receptor BRI1 (Wang et al., 2001), the CLV1 receptor in shoot meristem development (Clark et al., 1997) and the TMK1 receptor that is thought to sense auxin signaling (Dai et al., 2013; Xu et al., 2014). None of them showed discernable changes of DNA methylation in gene body and promoter regions (Fig. S5). Recently, the receptor-like kinase family SOMATIC EMBRYOGENESIS RECEPTOR KINASE (SERK), which has four members, was found to bind to ER receptors to regulate stomatal development (Meng et al., 2015). SERK3 (also called BAK1) interacts with BRI1 to mediate brassinosteroid signaling in *Arabidopsis* (Li et al., 2002; Nam and Li, 2002). Three SERKs (1, 2 and 3) seemed to be mildly hypermethylated in *ibm1* and *edm2* mutants (Fig. S6A). However, their transcription levels were apparently elevated as demonstrated by real-time PCR (Fig. S6B). Therefore, considering the important fact that *er ibm1* resembles *er*, the stomatal phenotypes of *ibm1* and *edm2* are not likely to be caused by elevated expression of SERK genes, but could be related to high DNA methylation and low transcription levels of ER genes.

cmt3 and *kyp* mutations are epistatic to *ibm1* and *edm2* in stomatal development

Previous reports showed that the ectopic cytosine methylation phenotype of *ibm1* depends on CMT3 DNA methyltransferase- and

Development (2016) 143, 4452-4461 doi:10.1242/dev.129932

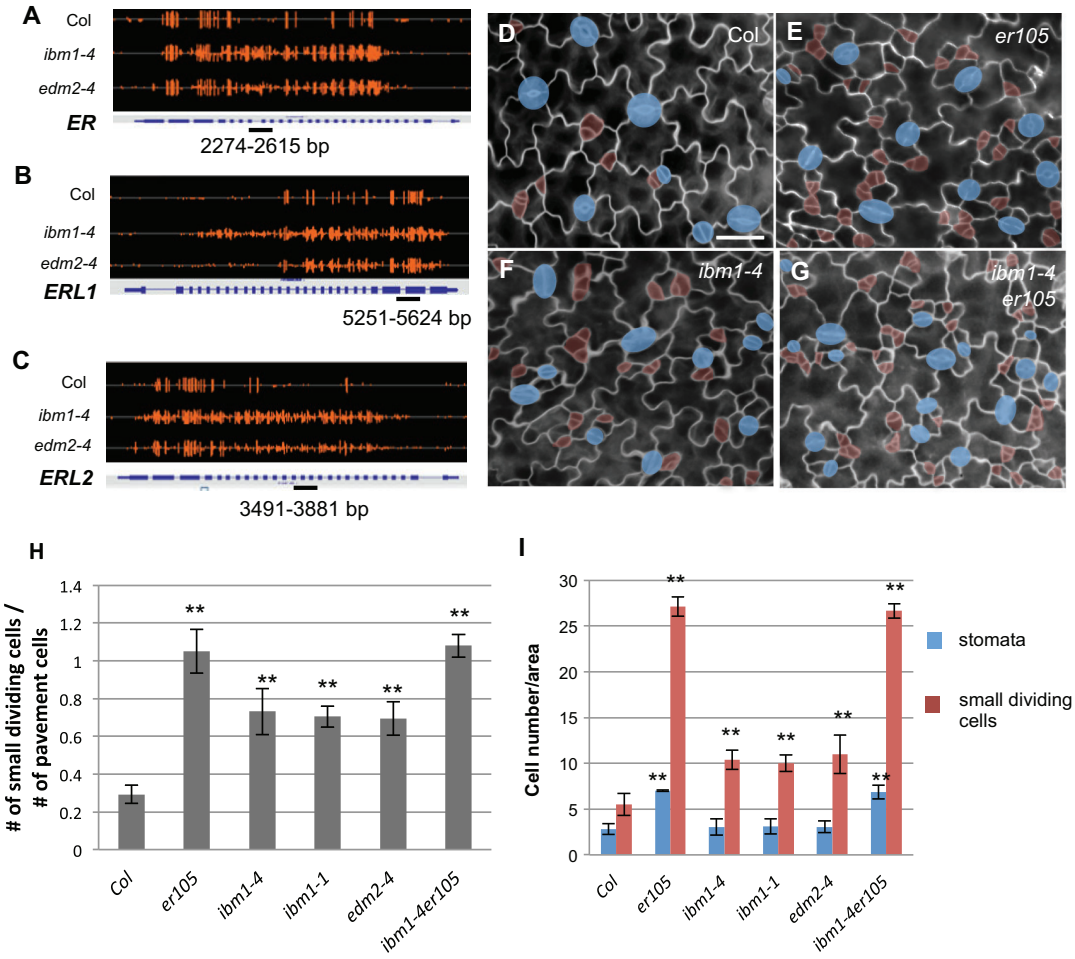

Fig. 4. ER genes are hypermethylated in *ibm1* and *edm2* mutants. (A-C) Integrated genome viewer snapshots showing the DNA methylation status of *ER* (A), *ERL1* (B) and *ERL2* (C) in the wild type (Col), and in *ibm1-4* and *edm2-4* mutants. Orange bars indicate the sites of cytosine methylation and the height of the bars indicates the relative DNA methylation level. The genomic regions where bisulfite sequencing was performed are underlined. (D-G) Epi-fluorescence images of 3-dpg adaxial cotyledon of Col (D), *er105* (E), *ibm1-4* (F) and *ibm1-4 er105* (G). The double mutant resembles *er105*. Cell outlines are marked by FM1-43 staining. Scale bar: 30 µm (in D, for D-G). The images in D and F are also shown in Fig. 1A and Fig. 1D, respectively, because these experiments were performed concurrently. (H) Histogram showing the ratio of the total number of small dividing cells relative to that of the pavement cells in different genotypes. (I) Quantification of the total number of stomata and small dividing cells. Data in H and I are mean±s.d. **P*<0.05, ***P*<0.01, compared with the wild type (Col) by Student's *t*-test with Bonferroni correction (*n*=6).

the KYP histone methyltransferase-mediated H3K9 dimethylation, and *cmt3* and *kyp* mutations suppressed almost all detectable developmental defects in *ibm1* mutants (Saze et al., 2008). Therefore, we crossed *ibm1* and *edm2* mutants with *kyp* and *cmt3* to create the corresponding double mutants (Fig. 6; Fig. 7). We found that, differing from the increased stomatal lineage divisions in *ibm1* and *edm2*, stomatal development and patterning of the single *kyp* and *cmt3* mutants were indistinguishable from the wild type (Col) (Fig. 6A-C). Furthermore, the double mutants *ibm1-4 kyp* and *ibm1-4 cmt3* did not exhibit the stomatal phenotype seen in *ibm1-4*, instead resembling those of *kyp*, *cmt3* and Col (Fig. 6D-F). Similar effects were also seen when another allele of *ibm1* was used (*ibm1-1 kyp*; Fig. S7A,B). These data suggested that both *KYP* and *CMT3* are required for the *ibm1*-induced stomatal phenotypes. Similarly, the double mutants of *edm2-5 kyp* and *edm2-4 cmt3* restored the stomatal phenotypes of *edm2-4* back to the wild-type level (Fig. 7).

To further support the hypothesis that the recovered stomatal phenotype, when *kyp* and *cmt* mutations were introgressed into *ibm1* mutant plants, is related to ER gene expression, we performed real-time PCR assays. Our data showed that the expression levels of *ER*, *ERL1* and *ERL2* were lower in *ibm1*, but when combined with the *kyp* and *cmt3* mutations, the decreased expression of the ER family genes recovered to near wild-type level in the double mutants of *ibm1 kyp* and *ibm1 cmt3* (Fig. 6H).

We also found that a loss-of-function mutation in the RdDM component AGO4 did not exhibit any obvious stomatal defects in division, production and patterning (Fig. S8A,B). As expected, *ago4* did not suppress the stomatal defects of the *ibm1* mutant (Fig. S8C-F) supporting the hypothesis that *ibm1* is epistatic to *ago4* in stomatal development (Fig. S9).

DISCUSSION

Hypermethylation of ER genes in *ibm1* and *edm2*

The whole-genome bisulfite sequencing data revealed increased DNA methylation levels in the coding regions of *ER*, *ERL1* and *ERL2* in *ibm1* and *edm2* mutants. Our individual locus bisulfite sequencing data confirmed that, in *ibm1* mutants, all three ER genes were hypermethylated, particularly at CHG sites (Fig. 5A-C). The suggestion that ER genes are putative targets

Development (2016) 143, 4452-4461 doi:10.1242/dev.129932

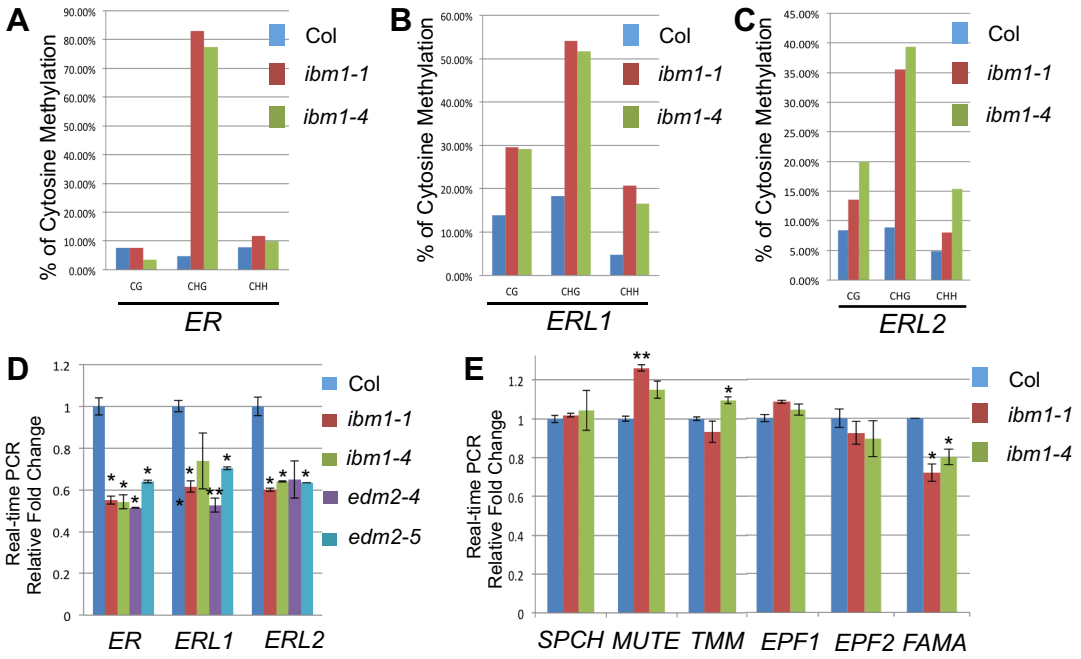

Fig. 5. The *ibm1* mutations affect the DNA methylation levels of ER genes. (A-C) Individual locus bisulfite sequencing analyses of CG, CHG, CHH methylation in *ER* (A), *ERL1* (B) and *ERL2* (C) in Col, *ibm1-1* and *ibm1-4*. At least ten clones were selected from each sample. Striking methylation elevation in CHGs was found in all three ER genes when *IBM1* is defective. (D,E) Transcript level of stomata-related genes in Col and in *ibm1* and *edm2* mutants. The expression of ER genes was suppressed in *ibm1* and *edm2* mutants. Values are mean±s.d. Data were collected from three biological replicates and the expression fold changes were normalized to the transcript level in Col. **P*<0.05, ***P*<0.01, compared with the wild type (Col) by Student's *t*-test with Bonferroni correction; *n*=3 replicates.

of IBM1 in stomatal development is consistent with the characteristics of the typical genes that are under the control of IBM1 in *Arabidopsis*. These genes often encode long transcripts (the full-length genomic region of ER is about 6 kb) and IBM1-mediated suppression of DNA methylation occurs mainly at CHG sites (Miura et al., 2009).

Many studies have investigated how ER receptor-like kinases play pleiotropic functions in plant development, physiological processes and responses to growth and environmental stimuli (Shpak, 2013; van Zanten et al., 2009), but not much is known about how expression patterns and levels of the *ER* gene are modulated. A recent study showed that 26 introns in the *ER* gene are important for its mRNA accumulation and efficient translation. It was hypothesized that these introns might affect the elongation of the poly(A) tail of *ER* mRNA or the assembly of a spliceosome that might promote *ER* transcription and translation (Karve et al., 2011). Here, we propose another possibility that these introns could recruit other regulatory factors, e.g. IBM1 and/or EDM2 chromatin factors, which antagonize histone modification- and DNA methylation-induced gene silencing for sustained expression of ER in plant development.

Epigenetic regulation of genes that modulate stomatal lineage population

Our study showed that the IBM1 H3K9me2 demethylase is necessary for preventing the gene body DNA methylation of three ER genes. DNA hypermethylation of the ER genes in *ibm1* mutants depended on the DNA methyltransferase CMT3, but not on the RdDM pathway. By contrast, it was recently reported that the DNA methylation level of *EPF2*, encoding a signal peptide that functions upstream of the ER receptors (Hunt and Gray, 2009), was controlled through another mechanism, the DNA demethylase ROS1 (Yamamuro et al., 2014). *ros1* loss-of-function mutants produced overproliferated stomatal lineage cells because the *EPF2* promoter was hypermethylated and silenced. The stomatal phenotype of *ros1* can be counteracted by RdDM mutations (Yamamuro et al., 2014). The CMT3 and RdDM pathways seemed to work in a specific manner on target genes; ER genes were hypermethylated in *ibm1* mutants, but not in *ros1* mutants (Fig. S11), and *EPF2* was hypermethylated in *ros1* mutants, but not in *ibm1* (Table S1). Taken together, the initiation and maintenance of the stomatal lineage cells, a specialized stem cell population in plants (Matos and Bergmann, 2014), are ensured by two independent mechanisms: ROS1-mediated DNA demethylation on the *EPF2* promoter and IBM1-mediated histone demethylation on the bodies of ER genes. These epigenetic mechanisms dramatically differ from those in mammalian pluripotent stem cells in which chromatin regulators mainly target and regulate pluripotency transcription factors (Luo et al., 2014; Papp and Plath, 2013). So far, no direct evidence supports the hypothesis that the key stomatal differentiation transcription factors SPCH, MUTE, FAMA and SCRM are under active DNA methylation control, though possible regulations of chromatin modifiers that enforce terminal guard cell integrity are emerging (Lee et al., 2014; Matos et al., 2014).

Expression pattern of *IBM1* and its effect on ER genes at the tissue level

It is interesting to note that, in *ibm1* and *edm2* mutants, the CHG hypermethylation in the genic regions of all three ER genes resulted in downregulation of their expression levels to about 50-60% of the wild-type level. The combined effect of three ER genes in *ibm1* seemed to produce relatively mild stomatal phenotypes, and no drastic developmental or patterning defects that might be detrimental to plant growth, in contrast to those found in *er erl1 erl2* triple mutants (Fig. S10; severe stomatal clustering and

Development (2016) 143, 4452-4461 doi:10.1242/dev.129932

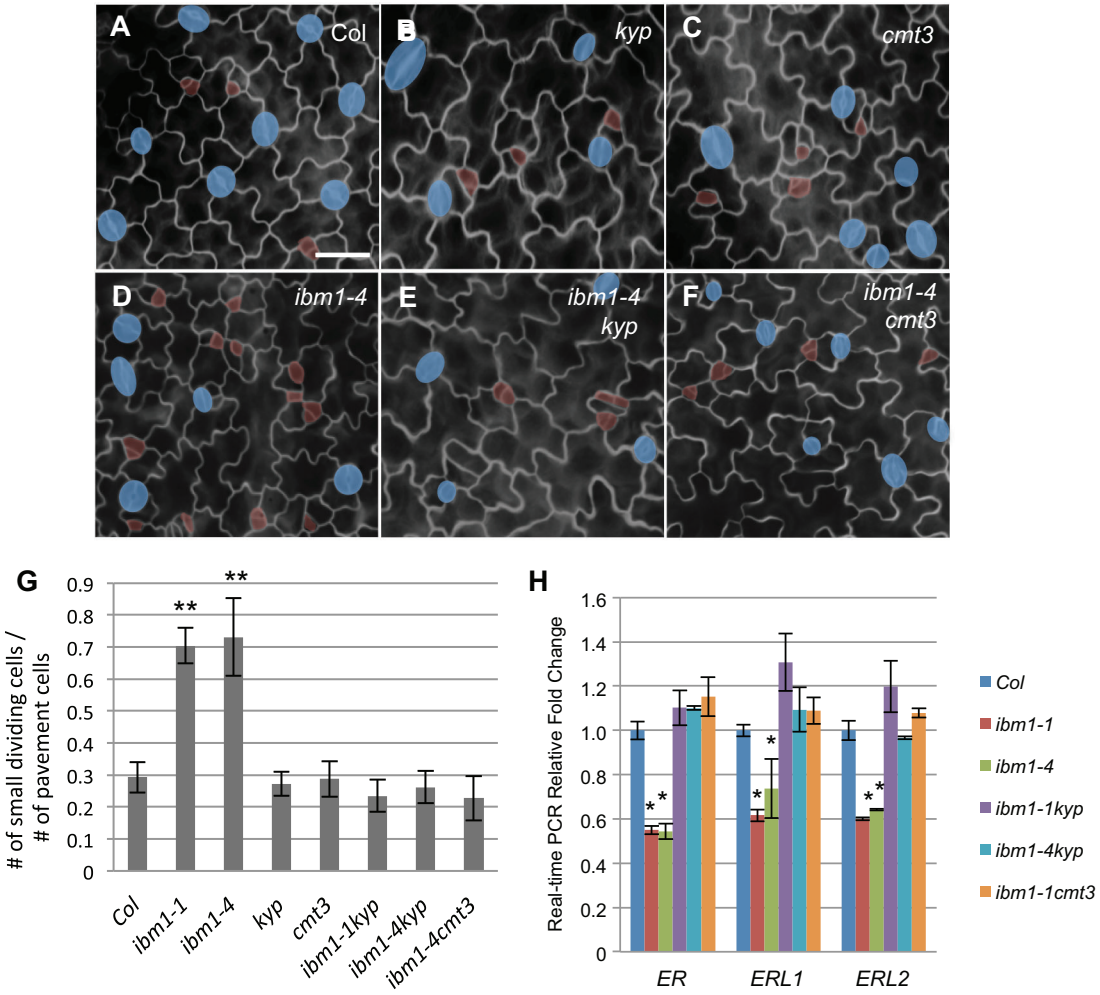

Fig. 6. *cmt3* and *kyp4* mutations suppress the stomatal defects in *ibm1* mutants. (A-F) Epi-fluorescence microscope images show 3-dpg adaxial cotyledons of Col (A), *kyp* (B), *cmt3* (C), *ibm1-4* (D), *ibm1-4 kyp* (E) and *ibm1-4 cmt3* (F). The control image (A) is also shown in Fig. 3A because these experiments were performed concurrently. Scale bar: 30 µm (in A, for A-F). *cmt3* and *kyp* were epistatic to *ibm1* mutations. (G) Histogram displaying the ratio of the total number of small dividing cells over that of the pavement cells in different mutant backgrounds. **P*<0.05, ***P*<0.01; one-way ANOVA with Bonferroni multiple comparison (*n*=6; ±s.d.). (H) Real-time PCR analyses for the expression level of ER genes in the indicated mutants. The expression fold changes were normalized to the transcript level in Col. Note the expression of ER genes recovered to the wild-type level when *kyp* and *cmt3* were intragressed into the *ibm1* mutants. **P*<0.05, ***P*< 0.01 compared with the wild type (Col) by Student's *t*-test with Bonferroni correction (*n*=3 replicates).

seedlings are lethal). Even when compared with the *er105* mutant, *ibm1* stomatal phenotypes are less severe (Fig. 4). These data seem to suggest that epigenetic factors (e.g. DNA methylation and histone modifications), compared with genetic disruptions, are more flexible and plastic in regulating gene expression.

Besides elevated stomatal lineage numbers, the *er* mutants also display prominent defects at the whole-plant level, including enlarged shoot apical meristem size (Mandel et al., 2014), short plant stature and compact inflorescence (Shpak, 2013; Torii et al., 1996). These phenotypes were not evident in *ibm1* and *edm2* mutants (Saze et al., 2008). We also found that the *IBM1* expression levels vary a lot in different tissues in *Arabidopsis* and the highest expression level of *IBM1-L* was found in inflorescences (Fig. S12). Our bisulfite sequencing data suggested that the *ER* gene was similarly hypermethylated in *ibm1* flowers (Fig. S13A,B), and the expression levels of the three ER genes were reduced (Fig. S13C). These data suggest that the absence of defects in inflorescence architecture in *ibm1* mutants might be explained by the small decrease in the levels of ER expression that were not sufficient to cause apical growth defects.

MATERIALS AND METHODS

Plant materials and growth conditions

The *Arabidopsis* homozygous loss-of-function mutants *ibm1-1* (point mutation) and *ibm1-4* (SALK_035608) were described previously (Saze et al., 2008). The third allele *ibm1-3* (SALK_023533) was a gift from Dr Ligeng Ma (College of Life Sciences, Capital Normal University, Beijing) *er105* and other mutants of the ER family were obtained from Dr Keiko Torii (Shpak et al., 2005). Other plant materials obtained from the *Arabidopsis* Biological Resource Center (http://www.arabidopsis.org) were confirmed by genotyping and sequencing. The ecotype Columbia (Col-0, labeled as Col in the figures and text) was used as the wild type unless otherwise noted. The *TMM* transcriptional marker was described by Nadeau and Sack (2002) and the *MUTE* promoter driving nuclear GFP was obtained from Dr Dominique Bergmann and used previously by Dong et al. (2009).

Arabidopsis seeds were sterilized with 5% household bleach solution and rinsed with sterilized double-distilled H_2O more than six times. Clean seeds were then dispersed on ½ MS (Murashige–Skoog) agar plates and incubated at 4°C for a day before being transferred to a standard plant growth chamber (23°C with16-h light/8-h dark cycles). When needed, seedlings were transferred to soil for continued growth under similar conditions.

Development (2016) 143, 4452-4461 doi:10.1242/dev.129932

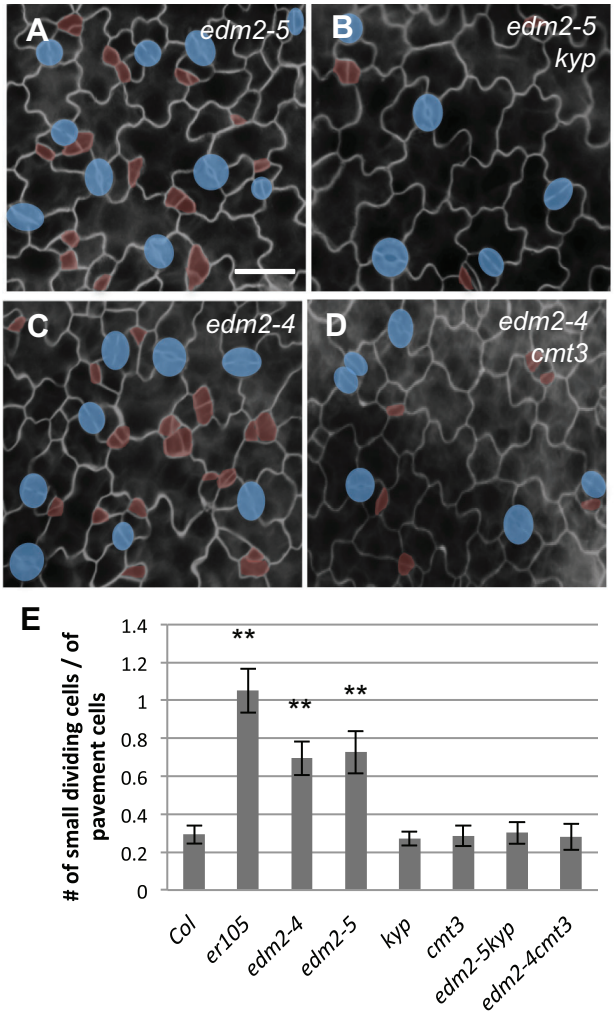

Fig. 7. *cmt3* and *kyp* mutations suppress the stomatal defects in *edm2* mutants. (A-D) Epi-fluorescence microscope images show 3-dpg adaxial cotyledons of *edm2-5* (A), *edm2-5 kyp* (B), *edm2-4* (C) and *edm2-4 cmt3* (D). Scale bar: 30 µm (in A, for A-D). *cmt3* and *kyp* were epistatic to *edm2* mutations. (E) Histogram displaying the ratio of the total number of small dividing cells over that of the pavement cells in different mutant backgrounds. **P*<0.05, ***P*<0.01; one-way ANOVA with Bonferroni multiple comparison (*n*=6; ±s.d.).

Microscopic observation and phenotype quantification

To examine stomatal phenotypes, *Arabidopsis* cotyledons (3-, 8- and 16-dpg) and true leaves (12-dpg) were stained with FM1-43 (Invitrogen T35356, 1 µg/ml), a fluorescent probe that integrates into the plasma membrane to outline cell shape. Seedlings were examined on an Olympus BX53 fluorescence microscope equipped with a GFP filter.

For quantification, the genetic materials used for counting cells in 3-dpg cotyledons were grown at the same time and under the same growth conditions to ensure the materials across the board are fully comparable in most of the figures. The stomatal lineage cells under division were counted as 'small dividing cells'. The epidermal cells are classified into three groups: pavement cells (larger than a mature guard cell and showing at least one obvious lobe), guard cells, and small dividing cells. To quantify stomatal phenotype, typically, cells from six independent cotyledons from six individual plants were collected for each sample. An area of 122,500 µm^2 (350×350 µm) from each sample was documented for cell counting. To test statistical significance, Student's *t*-test combined with Bonferroni correction was generally used. When more than two groups were compared, one-way ANOVA and Bonferroni multiple comparison were used.

To visualize *TMM* and *MUTE* transcriptional reporters (*TMMp-GFP* and *MUTEp-nucGFP*) in the *ibm1* mutants, a Leica SP5 confocal microscope was used to document the GFP expression pattern in the 3-dpg seedlings counterstained with FM4-64 (Invitrogen; F34653). The excitation/emission spectra were: GFP 488 nm/500-530 nm and FM4-64 561 nm/570-652 nm.

Identification of hypermethylated genes

The whole-genome bisulfite sequencing data we used for analyses were reported previously (Lei et al., 2014). To compare the DNA methylation level of each target gene related to stomatal development, their genomic sequences, including the promoter and the coding regions, were scanned for methylated cytosines in CG, CHG and CHH contexts. We collected the numbers of methylated cytosines in each context to indicate DNA methylations levels. These numbers were calculated and compared between the wild type (Col) and the related mutants (*ibm1*, *edm2* and others).

Real-time PCR

The RNeasy Plant Mini Kit (Qiagen) was used to extract total RNAs from 14-dpg *Arabidopsis* plants. After the removal of DNA, 1 µg of total RNAs served as template for synthesizing the first strand cDNAs with a One-Step SYBR PrimeScript RT-PCR Kit II (Perfect Real Time) (Takara). Real-time PCR was performed following the manufacturer's instructions. The first strand cDNA mixture was diluted four times and 2 µl was used as template in a 25 µl of PCR reaction with iQ SYBR Green Supermix (Bio-Rad). The PCR reactions were performed following this protocol: pre-incubation at 95°C for 5 min followed by 40 cycles of denaturation at 95°C for 15 s, annealing at 56°C for 30 s, and extension at 72°C for 30 s. The primers used are listed in Table S2. Reactions were carried out on a iQ5 Multicolour Real-Time PCR Detection System (Bio-Rad). The comparative threshold cycle (Ct) method was used to determine the relative transcript levels and the expression levels of *ACTIN2* were used as an internal control.

Individual locus bisulfite sequencing

The genomic DNA of *Arabidopsis* plants (14-dpg) was extracted by a DNeasy Plant Mini Kit (Qiagen). About 600 ng of genomic DNAs were aliquoted for each cytosine conversion reaction, which is achieved by using an Epitect Bisulfite Kit (Qiagen) and following the manufacturer's instructions. Out of 25 µl of the reaction mixture, 2 µl of bisulfite-treated DNA was used for nested PCR, which was programmed as follows: initial denaturation at 94°C for 3 min followed by 40 cycles of denaturation at 95°C for 15 s, annealing at 58°C for 30 s, and extension 72°C for 40 s using an ExTaq DNA polymerase (Takara). The resulting PCR products were ligated to pMD18-T vector (Takara) following the manufacturer's instructions. At least 15 clones were picked for sequencing to determine the DNA methylation level at each tested region.

Acknowledgements

We thank Jian Liang and Cheng Zhao for their technical support at the PSC and Dr Honggui La for helpful discussion.

Competing interests

The authors declare no competing or financial interests.

Author contributions

Y.W. and X.X performed experiments and analyzed data. Y.W., J.D. and J.-K.Z. designed experiments and wrote the manuscript.

Funding

This research project was supported by funding from the Chinese Academy of Sciences; and grants from the National Institute of General Medical Sciences [R01 GM070795, R01 GM059138 and R01 GM109080]. Deposited in PMC for release after 12 months.

Supplementary information

Supplementary information available online at
http://dev.biologists.org/lookup/doi/10.1242/dev.129932.supplemental

References

Badeaux, A. I. and Shi, Y. (2013). Emerging roles for chromatin as a signal integration and storage platform. *Nat. Rev. Mol. Cell Biol.* **14**, 211-224.

Bartee, L., Malagnac, F. and Bender, J. (2001). Arabidopsis cmt3 chromomethylase mutations block non-CG methylation and silencing of an endogenous gene. *Genes Dev.* **15**, 1753-1758.

Clark, S. E., Williams, R. W. and Meyerowitz, E. M. (1997). The CLAVATA1 gene encodes a putative receptor kinase that controls shoot and floral meristem size in Arabidopsis. *Cell* **89**, 575-585.
Dai, N., Wang, W., Patterson, S. E. and Bleecker, A. B. (2013). The TMK subfamily of receptor-like kinases in Arabidopsis display an essential role in growth and a reduced sensitivity to auxin. *PLoS ONE* **8**, e60990.
Dong, J., MacAlister, C. A. and Bergmann, D. C. (2009). BASL controls asymmetric cell division in Arabidopsis. *Cell* **137**, 1320-1330.
Ebbs, M. L., Bartee, L. and Bender, J. (2005). H3 lysine 9 methylation is maintained on a transcribed inverted repeat by combined action of SUVH6 and SUVH4 methyltransferases. *Mol. Cell. Biol.* **25**, 10507-10515.
Eulgem, T., Tsuchiya, T., Wang, X.-J., Beasley, B., Cuzick, A., Tör, M., Zhu, T., McDowell, J. M., Holub, E. and Dangl, J. L. (2007). EDM2 is required for RPP7-dependent disease resistance in Arabidopsis and affects RPP7 transcript levels. *Plant J.* **49**, 829-839.
Fan, D., Dai, Y., Wang, X., Wang, Z., He, H., Yang, H., Cao, Y., Deng, X. W. and Ma, L. (2012). IBM1, a JmjC domain-containing histone demethylase, is involved in the regulation of RNA-directed DNA methylation through the epigenetic control of RDR2 and DCL3 expression in Arabidopsis. *Nucleic Acids Res.* **40**, 8905-8916.
Fuks, F. (2005). DNA methylation and histone modifications: teaming up to silence genes. *Curr. Opin. Genet. Dev.* **15**, 490-495.
Hara, K., Kajita, R., Torii, K. U., Bergmann, D. C. and Kakimoto, T. (2007). The secretory peptide gene EPF1 enforces the stomatal one-cell-spacing rule. *Genes Dev.* **21**, 1720-1725.
Hara, K., Yokoo, T., Kajita, R., Onishi, T., Yahata, S., Peterson, K. M., Torii, K. U. and Kakimoto, T. (2009). Epidermal cell density is autoregulated via a secretory peptide, EPIDERMAL PATTERNING FACTOR 2 in Arabidopsis leaves. *Plant Cell Physiol.* **50**, 1019-1031.
He, X. J., Chen, T. and Zhu, J. K. (2011). Regulation and function of DNA methylation in plants and animals. *Cell Res.* **21**, 442-465.
Hunt, L. and Gray, J. E. (2009). The signaling peptide EPF2 controls asymmetric cell divisions during stomatal development. *Curr. Biol.* **19**, 864-869.
Inagaki, S., Miura-Kamio, A., Nakamura, Y., Lu, F., Cui, X., Cao, X., Kimura, H., Saze, H. and Kakutani, T. (2010). Autocatalytic differentiation of epigenetic modifications within the Arabidopsis genome. *EMBO J.* **29**, 3496-3506.
Jackson, J. P., Lindroth, A. M., Cao, X. and Jacobsen, S. E. (2002). Control of CpNpG DNA methylation by the KRYPTONITE histone H3 methyltransferase. *Nature* **416**, 556-560.
Kanaoka, M. M., Pillitteri, L. J., Fujii, H., Yoshida, Y., Bogenschutz, N. L., Takabayashi, J., Zhu, J.-K. and Torii, K. U. (2008). SCREAM/ICE1 and SCREAM2 specify three cell-state transitional steps leading to arabidopsis stomatal differentiation. *Plant Cell* **20**, 1775-1785.
Karve, R., Liu, W., Willet, S. G., Torii, K. U. and Shpak, E. D. (2011). The presence of multiple introns is essential for ERECTA expression in Arabidopsis. *RNA* **17**, 1907-1921.
Klose, R. J., Kallin, E. M. and Zhang, Y. (2006). JmjC-domain-containing proteins and histone demethylation. *Nat. Rev. Genet.* **7**, 715-727.
Kondo, T., Kajita, R., Miyazaki, A., Hokoyama, M., Nakamura-Miura, T., Mizuno, S., Masuda, Y., Irie, K., Tanaka, Y., Takada, S. et al. (2010). Stomatal density is controlled by a mesophyll-derived signaling molecule. *Plant Cell Physiol.* **51**, 1-8.
Lai, L. B., Nadeau, J. A., Lucas, J., Lee, E. K., Nakagawa, T., Zhao, L., Geisler, M. and Sack, F. D. (2005). The Arabidopsis R2R3 MYB proteins FOUR LIPS and MYB88 restrict divisions late in the stomatal cell lineage. *Plant Cell* **17**, 2754-2767.
Lampard, G. R., Lukowitz, W., Ellis, B. E. and Bergmann, D. C. (2009). Novel and expanded roles for MAPK signaling in Arabidopsis stomatal cell fate revealed by cell type-specific manipulations. *Plant Cell* **21**, 3506-3517.
Lau, O. S. and Bergmann, D. C. (2012). Stomatal development: a plant's perspective on cell polarity, cell fate transitions and intercellular communication. *Development* **139**, 3683-3692.
Law, J. A. and Jacobsen, S E. (2010). Establishing, maintaining and modifying DNA methylation patterns in plants and animals. *Nat. Rev. Genet.* **11**, 204-220.
Lee, E. K., Lucas, J. R., Goodrich, J. and Sack, F. D. (2014). Arabidopsis guard cell integrity involves the epigenetic stabilization of the FLP and FAMA transcription factor genes. *Plant J.* **78**, 566-577.
Lei, M., La, H., Lu, K., Wang, P., Miki, D., Ren, Z., Duan, C.-G., Wang, X., Tang, K., Zeng, L. et al. (2014). Arabidopsis EDM2 promotes IBM1 distal polyadenylation and regulates genome DNA methylation patterns. *Proc. Natl. Acad. Sci. USA* **111**, 527-532.
Li, J., Wen, J., Lease, K. A., Doke, J. T., Tax, F. E. and Walker, J. C. (2002). BAK1, an Arabidopsis LRR receptor-like protein kinase, interacts with BRI1 and modulates brassinosteroid signaling. *Cell* **110**, 213-222.
Lindroth, A. M., Cao, X., Jackson, J. P., Zilberman, D., McCallum, C. M., Henikoff, S. and Jacobsen, S. E. (2001). Requirement of CHROMOMETHYLASE3 for maintenance of CpXpG methylation. *Science* **292**, 2077-2080.
Liu, C., Lu, F., Cui, X. and Cao, X. (2010). Histone methylation in higher plants. *Annu. Rev. Plant Biol.* **61**, 395-420.
Luo, C., Dong, J., Zhang, Y. and Lam, E. (2014). Decoding the role of chromatin architecture in development: coming closer to the end of the tunnel. *Front. Plant Sci.* **5**, 374.
MacAlister, C. A., Ohashi-Ito, K. and Bergmann, D. C. (2007). Transcription factor control of asymmetric cell divisions that establish the stomatal lineage. *Nature* **445**, 537-540.
Malagnac, F., Bartee, L. and Bender, J. (2002). An Arabidopsis SET domain protein required for maintenance but not establishment of DNA methylation. *EMBO J.* **21**, 6842-6852.
Mandel, T., Moreau, F., Kutsher, Y., Fletcher, J. C., Carles, C. C. and Eshed Williams, L. (2014). The ERECTA receptor kinase regulates Arabidopsis shoot apical meristem size, phyllotaxy and floral meristem identity. *Development* **141**, 830-841.
Matos, J. L. and Bergmann, D. C. (2014). Convergence of stem cell behaviors and genetic regulation between animals and plants: insights from the Arabidopsis thaliana stomatal lineage. *F1000Prime Rep.* **6**, 53.
Matos, J. L., Lau, O. S., Hachez, C., Cruz-Ramírez, A., Scheres, B. and Bergmann, D. C. (2014). Irreversible fate commitment in the Arabidopsis stomatal lineage requires a FAMA and RETINOBLASTOMA-RELATED module. *ELife* **3**.
Matzke, M. A., Kanno, T. and Matzke, A. J. (2015). RNA-directed DNA methylation: The evolution of a complex epigenetic pathway in flowering plants. *Annu. Rev. Plant Biol.* **266**, 243-267.
Meng, X., Chen, X., Mang, H., Liu, C., Yu, X., Gao, X., Torii, K. U., He, P. and Shan, L. (2015). Differential function of Arabidopsis SERK family receptor-like kinases in stomatal patterning. *Curr. Biol.* **25**, 2361-2372.
Miura, A., Nakamura, M., Inagaki, S., Kobayashi, A., Saze, H. and Kakutani, T. (2009). An Arabidopsis jmjC domain protein protects transcribed genes from DNA methylation at CHG sites. *EMBO J.* **28**, 1078-1086.
Nadeau, J. A. and Sack, F. D. (2002). Control of stomatal distribution on the Arabidopsis leaf surface. *Science* **296**, 1697-1700.
Nam, K. H. and Li, J. (2002). BRI1/BAK1, a receptor kinase pair mediating brassinosteroid signaling. *Cell* **110**, 203-212.
Ohashi-Ito, K. and Bergmann, D. C. (2006). Arabidopsis FAMA controls the final proliferation/differentiation switch during stomatal development. *Plant Cell* **18**, 2493-2505.
Papp, B. and Plath, K. (2013). Epigenetics of reprogramming to induced pluripotency. *Cell* **152**, 1324-1343.
Pillitteri, L. J. and Dong, J. (2013). Stomatal development in Arabidopsis. *Arabidopsis Book* **11**, e0162.
Pillitteri, L. J. and Torii, K. U. (2012). Mechanisms of stomatal development. *Annu. Rev. Plant Biol.* **63**, 591-614.
Pillitteri, L. J., Sloan, D. B., Bogenschutz, N. L. and Torii, K. U. (2007). Termination of asymmetric cell division and differentiation of stomata. *Nature* **445**, 501-505.
Rowe, M. H. and Bergmann, D. C. (2010). Complex signals for simple cells: the expanding ranks of signals and receptors guiding stomatal development. *Curr. Opin. Plant Biol.* **13**, 548-555.
Saze, H., Shiraishi, A., Miura, A. and Kakutani, T. (2008). Control of genic DNA methylation by a jmjC domain-containing protein in Arabidopsis thaliana. *Science* **319**, 462-465.
Shiu, S.-H. and Bleecker, A. B. (2001). Receptor-like kinases from Arabidopsis form a monophyletic gene family related to animal receptor kinases. *Proc. Natl. Acad. Sci. USA* **98**, 10763-10768.
Shpak, E.-D. (2013). Diverse roles of ERECTA family genes in plant development. *J. Integr. Plant Biol.* **55**, 1238-1250.
Shpak, E. D., Berthiaume, C. T., Hill, E. J. and Torii, K. U. (2004). Synergistic interaction of three ERECTA-family receptor-like kinases controls Arabidopsis organ growth and flower development by promoting cell proliferation. *Development* **131**, 1491-1501.
Shpak, E. D., McAbee, J. M., Pillitteri, L. J. and Torii, K. U. (2005). Stomatal patterning and differentiation by synergistic interactions of receptor kinases. *Science* **309**, 290-293.
Sugano, S. S., Shimada, T., Imai, Y., Okawa, K., Tamai, A., Mori, M. and Hara-Nishimura, I. (2010). Stomagen positively regulates stomatal density in Arabidopsis. *Nature* **463**, 241-244.
Torii, K. U. (2012). Mix-and-match: ligand-receptor pairs in stomatal development and beyond. *Trends Plant Sci.* **17**, 711-719.
Torii, K. U., Mitsukawa, N., Oosumi, T., Matsuura, Y., Yokoyama, R., Whittier, R. F. and Komeda, Y. (1996). The Arabidopsis ERECTA gene encodes a putative receptor protein kinase with extracellular leucine-rich repeats. *Plant Cell* **8**, 735-746.
Tsuchiya, T. and Eulgem, T. (2010a). The Arabidopsis defense component EDM2 affects the floral transition in an FLC-dependent manner. *Plant J.* **62**, 518-528.
Tsuchiya, T. and Eulgem, T. (2010b). Co-option of EDM2 to distinct regulatory modules in Arabidopsis thaliana development. *BMC Plant Biol.* **10**, 203.

Development (2016) 143, 4452-4461 doi:10.1242/dev.129932

van Zanten, M., Snoek, L. B., Proveniers, M. C. G. and Peeters, A. J. (2009). The many functions of ERECTA. *Trends Plant Sci.* **14**, 214-218.

Wang, Z.-Y., Seto, H., Fujioka, S., Yoshida, S. and Chory, J. (2001). BRI1 is a critical component of a plasma-membrane receptor for plant steroids. *Nature* **410**, 380-383.

Wang, H., Ngwenyama, N., Liu, Y., Walker, J. C. and Zhang, S. (2007). Stomatal development and patterning are regulated by environmentally responsive mitogen-activated protein kinases in Arabidopsis. *Plant Cell* **19**, 63-73.

Wierzbicki, A. T., Haag, J. R. and Pikaard, C. S. (2008). Noncoding transcription by RNA polymerase Pol IVb/Pol V mediates transcriptional silencing of overlapping and adjacent genes. *Cell* **135**, 635-648.

Xu, T., Dai, N., Chen, J., Nagawa, S., Cao, M., Li, H., Zhou, Z., Chen, X., De Rycke, R., Rakusova, H. et al. (2014). Cell surface ABP1-TMK auxin-sensing complex activates ROP GTPase signaling. *Science* **343**, 1025-1028.

Yamamuro, C., Miki, D., Zheng, Z., Ma, J., Wang, J., Yang, Z., Dong, J. and Zhu, J.-K. (2014). Overproduction of stomatal lineage cells in Arabidopsis mutants defective in active DNA demethylation. *Nat. Commun.* **5**, 4062.

Zhang, H. and Zhu, J. K. (2011). RNA-directed DNA methylation. *Curr. Opin. Plant Biol.* **14**, 142-147.

Zheng, B., Wang, Z., Li, S., Yu, B., Liu, J.-Y. and Chen, X. (2009). Intergenic transcription by RNA polymerase II coordinates Pol IV and Pol V in siRNA-directed transcriptional gene silencing in Arabidopsis. *Genes Dev.* **23**, 2850-2860.

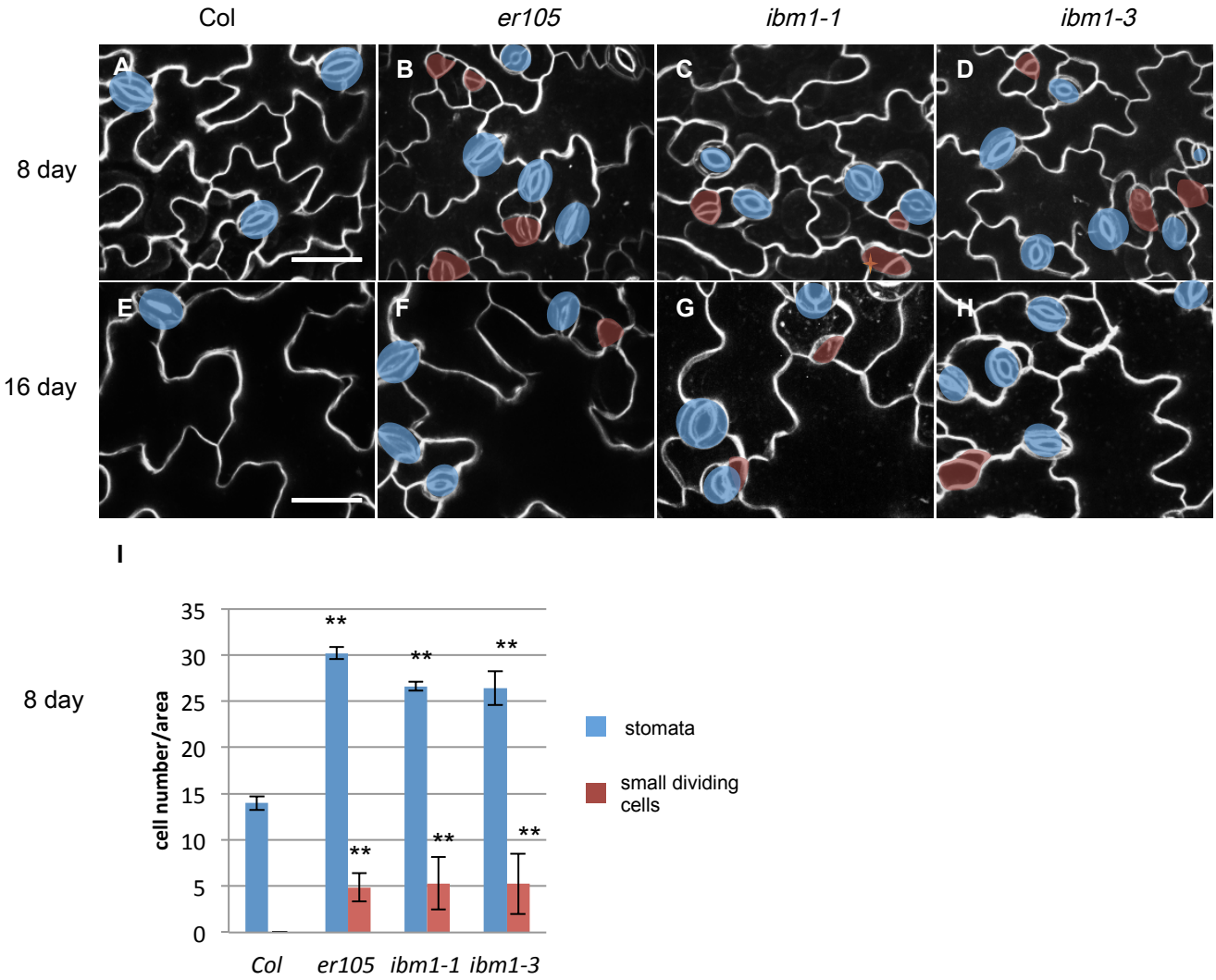

Fig. S1. Stomatal phenotype in mature cotyledons.
(A-D) Confocal images with multi-view acquisition to show 8-dpg adaxial cotyledons. Red shades mark stomatal lineage divisions. Blue shades highlights stomatal guard cells.
(E-H) Confocal images of 16-dpg adaxial, fully expanded cotyledons. At both stages, Col plants no longer produce stomatal lineage divisions (A and E), but *er105* (B and F) and *ibm* mutants (C, D, G and H) keep generating new divisions. Scale bars in A and E are 20 μm.
(I) Quantification of the number of stomata and small cells. Values are means ± SD. Data are collected from same sized areas (1024 x 1024 μm^2, n = 6 individual cotyledons for each line) . Significant differences * $P < 0.05$, ** $P < 0.01$; Student's *t*-test with Bonferroni Correction was used to compare the mutant values to those of Col.

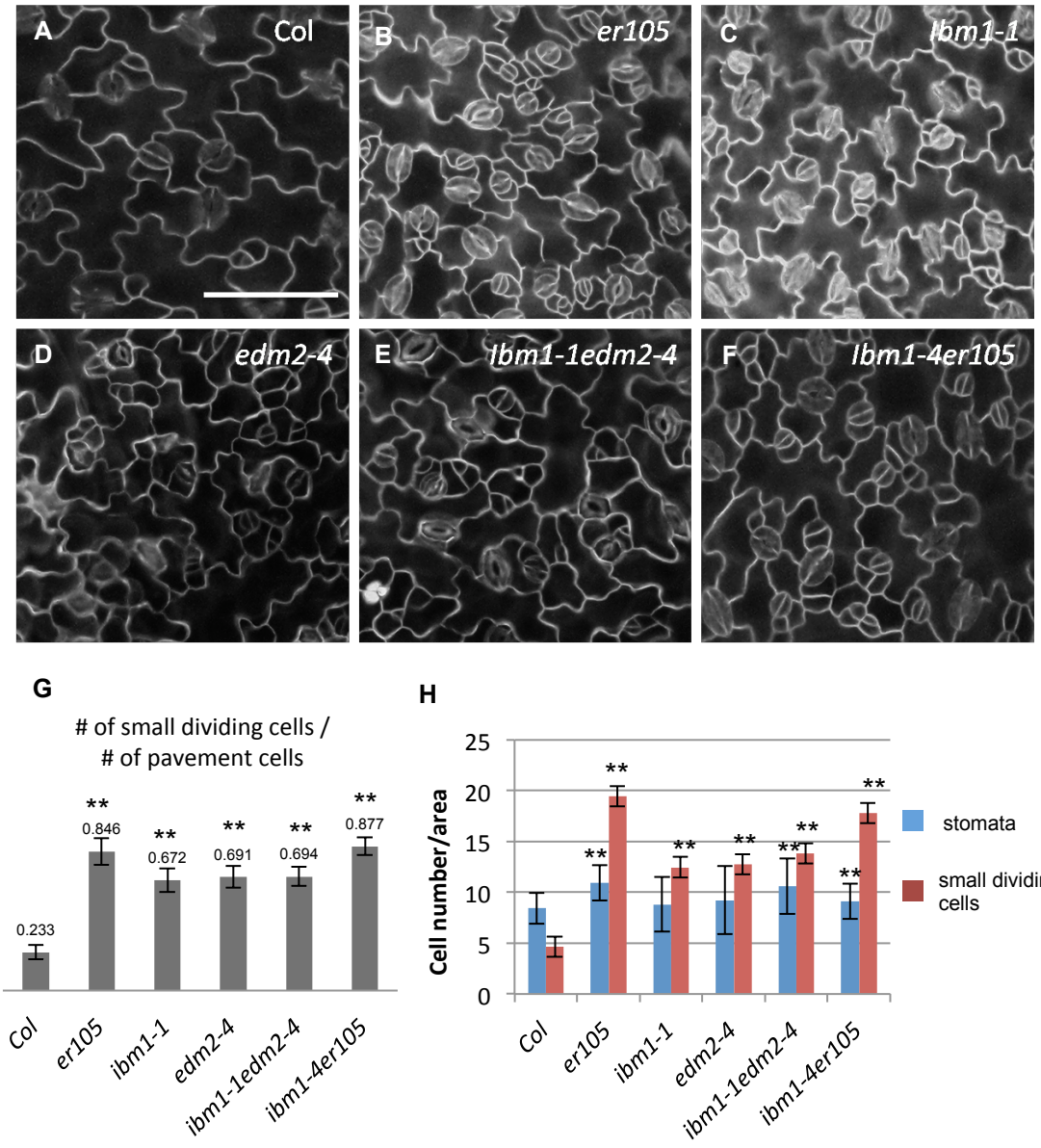

Fig. S2. Stomatal phenotype in 12-dpg true leaves.
(A-F) Confocal images to show 12-dpg abaxial true leaves of the designated genotypes. Scale bar in A = 20 μm. Others are at the same scale.
(G-H) Histograms show the ratio of total number of small dividing cells relative to that of pavement cells in different genotypes (G) and quantification of stomata and small dividing cells in indicated plants (H). For each sample, cells were counted from similarly positioned areas of 122,500 μm^2 in 12-dpg true leaves. Values are means ± SD, n = 6 individual leaves for each line. Significant differences * $P < 0.05$, ** $P < 0.01$; Student's *t*-test with Bonferroni Correction was used to compare the mutant values to those of Col.

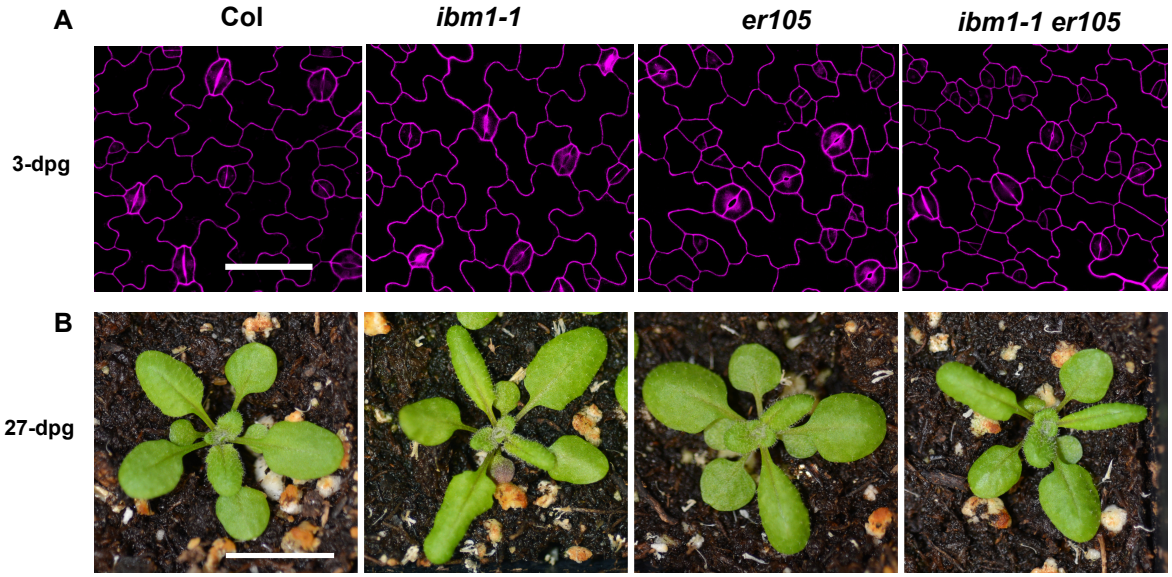

Fig. S3. Phenotypic comparison of *ibm1*, *er105* and the double mutant *ibm1-1 er105*.
(A) Confocal images of 3-dpg cotyledons. Cells were outlined by propidium iodide staining (magenta). Scale bar = 25 µm. The double mutant *ibm1-1 er105* is similar to *er105* in stomatal development and patterning.
(B) 27-day old plants of WT (Col), *ibm1-1, er105* and *ibm1-1 er105*. Scale bar in Col = 1 cm and others are at the same scale. The double mutant *ibm1-1 er105* is similar to *er105* in leaf shape and whole plant stature.

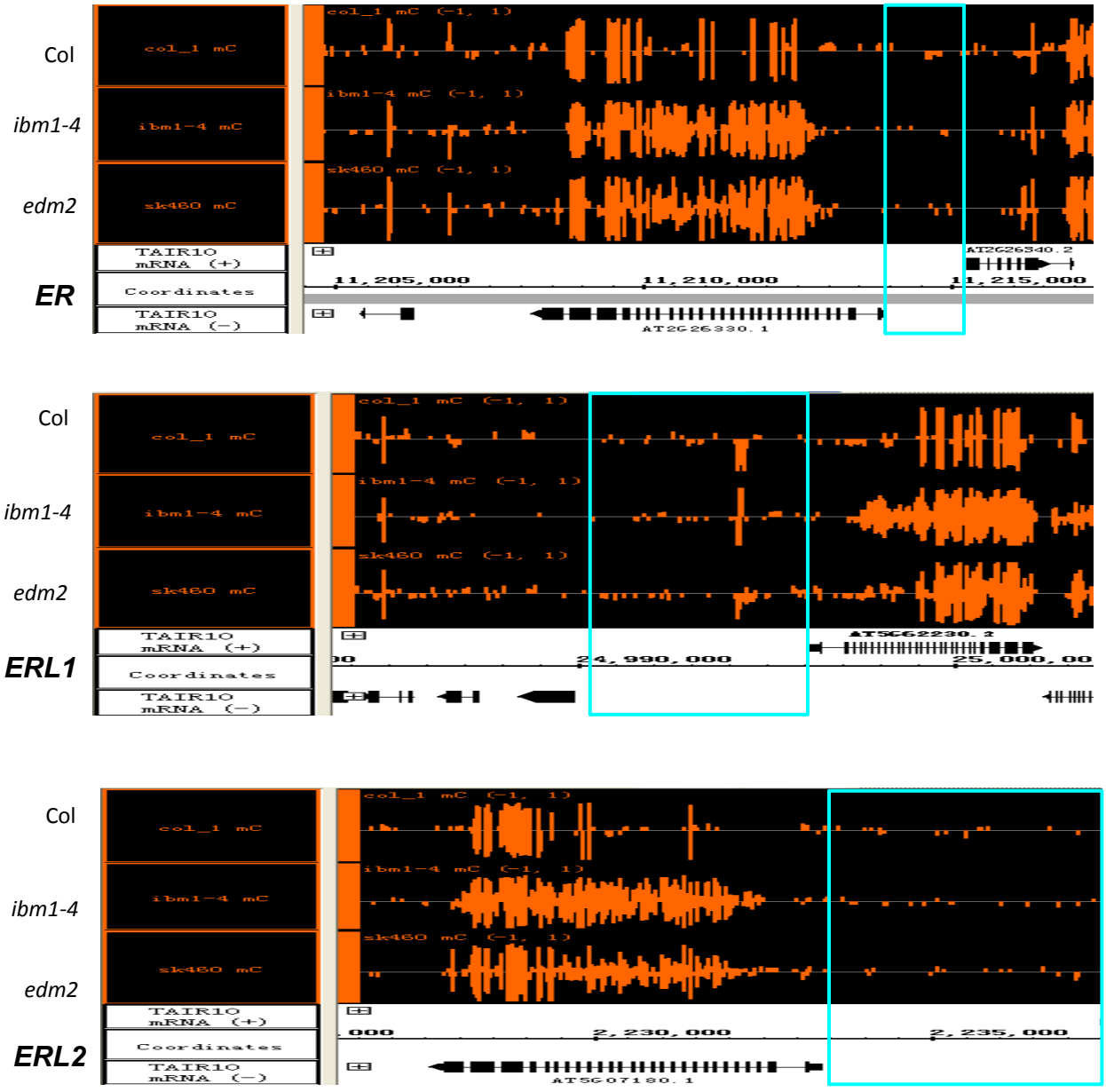

Fig. S4. The promoters of *ER* genes are not hypermethylated in *ibm1* mutants.

Integrated genome viewer shows the whole genome bisulfite sequencing of *ER* gene (top), *ERL1* (middle) and *ERL2* (bottom) in the wild-type (Col), *ibm1-4*, and *edm2* mutants. Cyan boxes label the promoter regions.

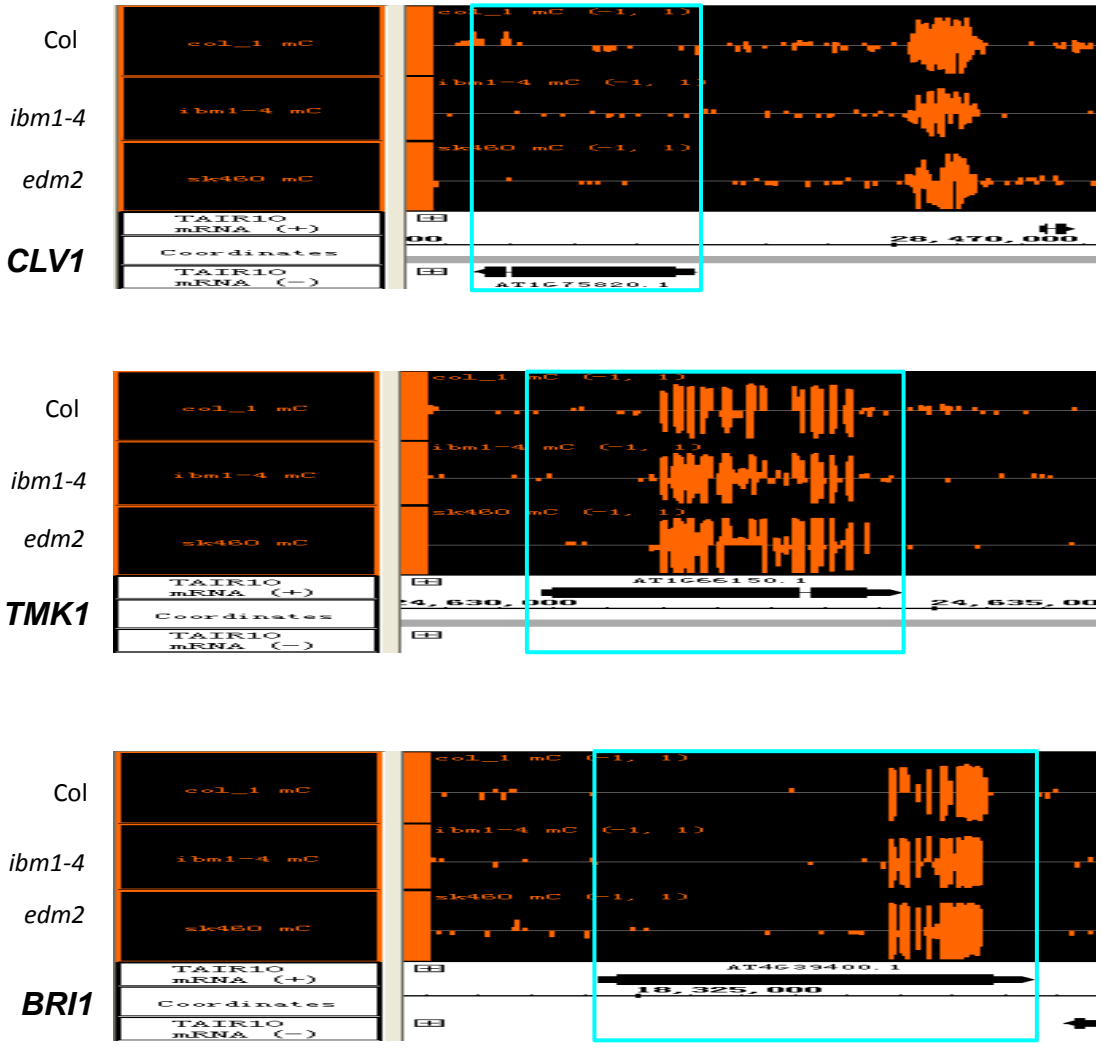

Fig. S5. Other receptor-like kinase genes are not significantly hypermethylated in *ibm1* mutants.
Integrated genome viewer shows the whole genome bisulfite sequencing data of *CLV1* (top), *TMK1* (middle) and *BRI1* (bottom) receptor-like kinase genes in the wild-type (Col), *ibm1-4*, and *edm2* mutants. Cyan boxes indicate the respective gene body regions.

A

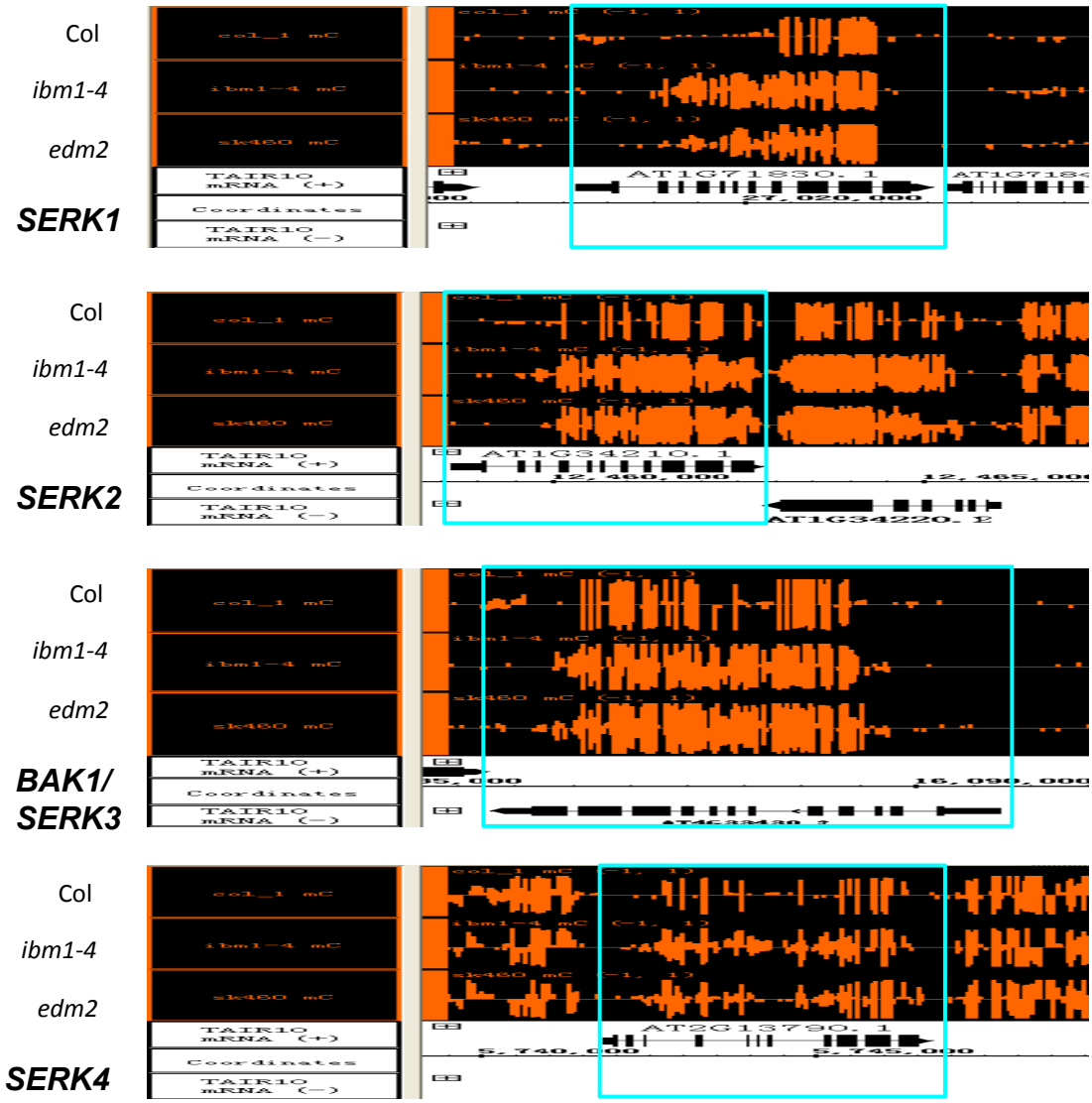

B

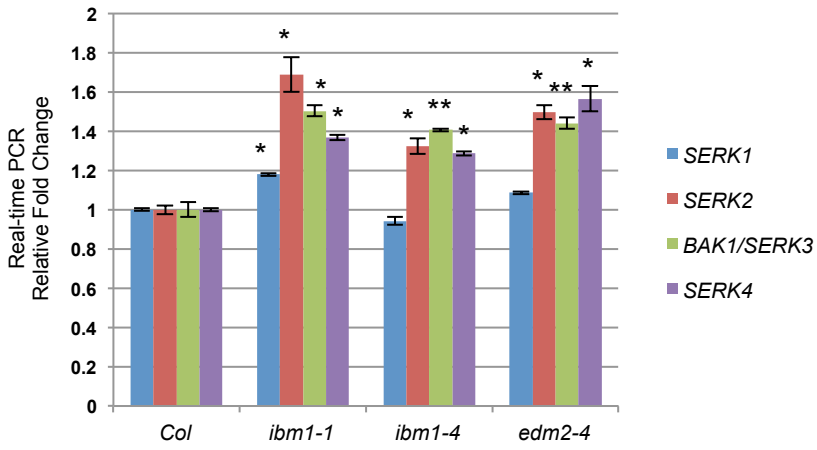

Fig. S6. Some SERK receptors are hypermethylated but expression are elevated in *ibm1* and *edm2* mutants

(A) Integrated genome viewer shows the whole genome bisulfite sequencing data of *SERK1*, *SERK2*, *BAK1/SERK3* and *SERK4* in the wild-type (Col), *ibm1-4*, and *edm2* mutants. Cyan boxes indicate the respective gene body regions. Gene body methylation is elevated in *SERK1*, *SERK2* and *BAK1/SERK3* genes, but not obvious in *SERK4* gene.

(B) Real-time PCR analyses of SERKs' expression in indicated plants. The expression fold changes were normalized to the transcription level of Col. Elevated expression levels of *SERK2, 3* and *4* were identified. Data were collected from three replicates. Significant differences * $P < 0.05$, ** $P < 0.01$; Student's *t*-test with Bonferroni Correction was used to compare the mutant values to those of Col (n = 3 replicates; ± SD) .

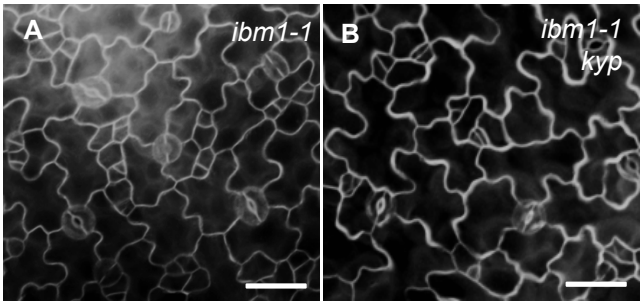

Fig. S7. *kyp* is epistatic to *ibm1*.
(A-B) Epi-fluorescent microscope images show 3-dpg adaxial codyledons of *ibm1-1* (A) and *ibm1-1 kyp.* The stomatal phenotype of *ibm1-1 kyp* is recovered to the wild-type level (quantification in Fig. 6). Cell outlines were marked by FM1-43 staining. Scale bars = 30 μm.

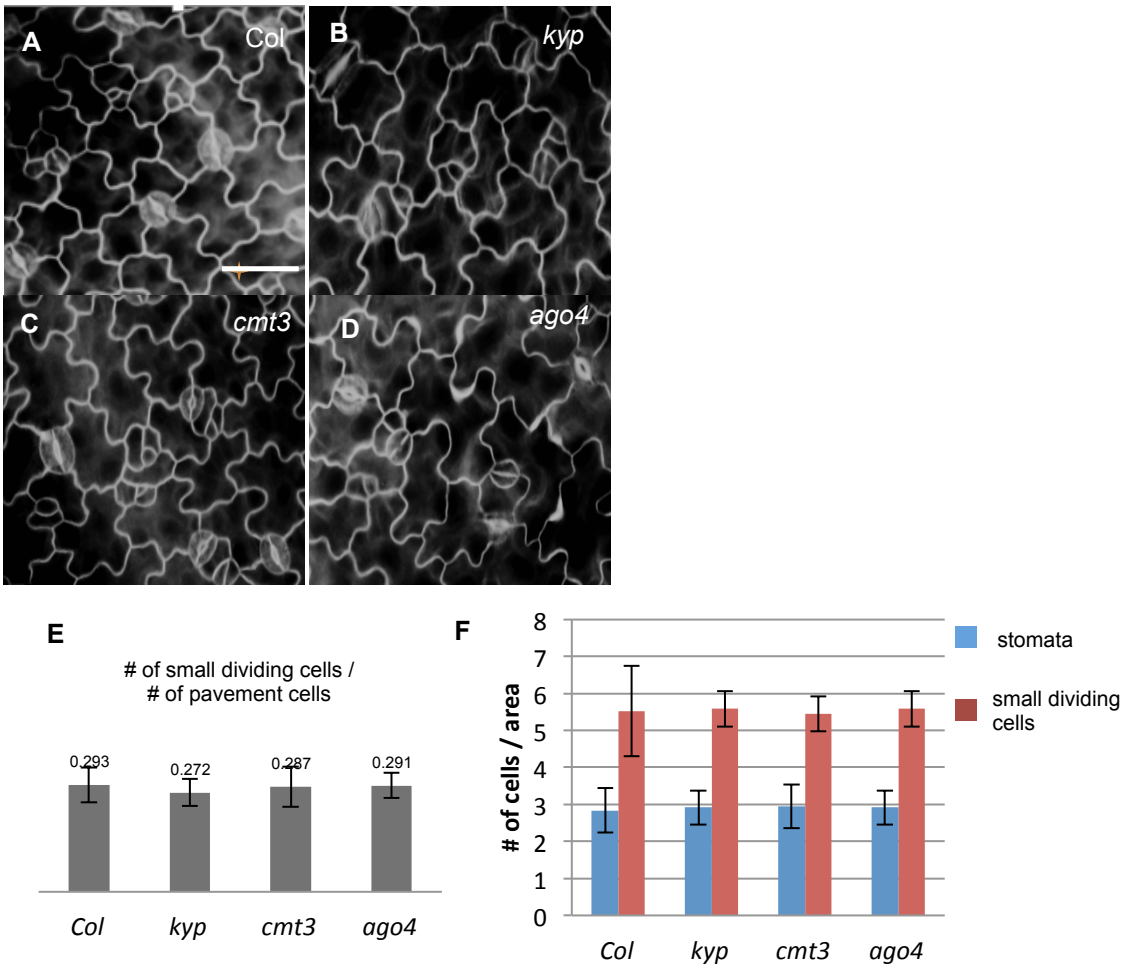

Fig. S8. Stomatal development and patterning in *kyp, cmt3* and *ago4* mutants.

(A-D) Epi-fluorescent microscope images show 3-dpg adaxial codyledons of Col (A), *kyp* (B), *cmt3* (C) and *ago4* (D). They are all very similar to Col. Cell outlines were marked by FM1-43 staining (green). Scale bars in (A) = 30 μm. Others are at the same scale.

(E) Histogram shows the ratio of the total number of small dividing cells relative to that of the pavement cells in different genotypes.

(F) Quantification of the number of stomata and small dividing cells collected from same sized areas. Values in (E-F) are means ± SD, n = 6 individual cotyledons for each line. No significant differences were detected by one-way ANOVA with Bonferroni multiple comparison.

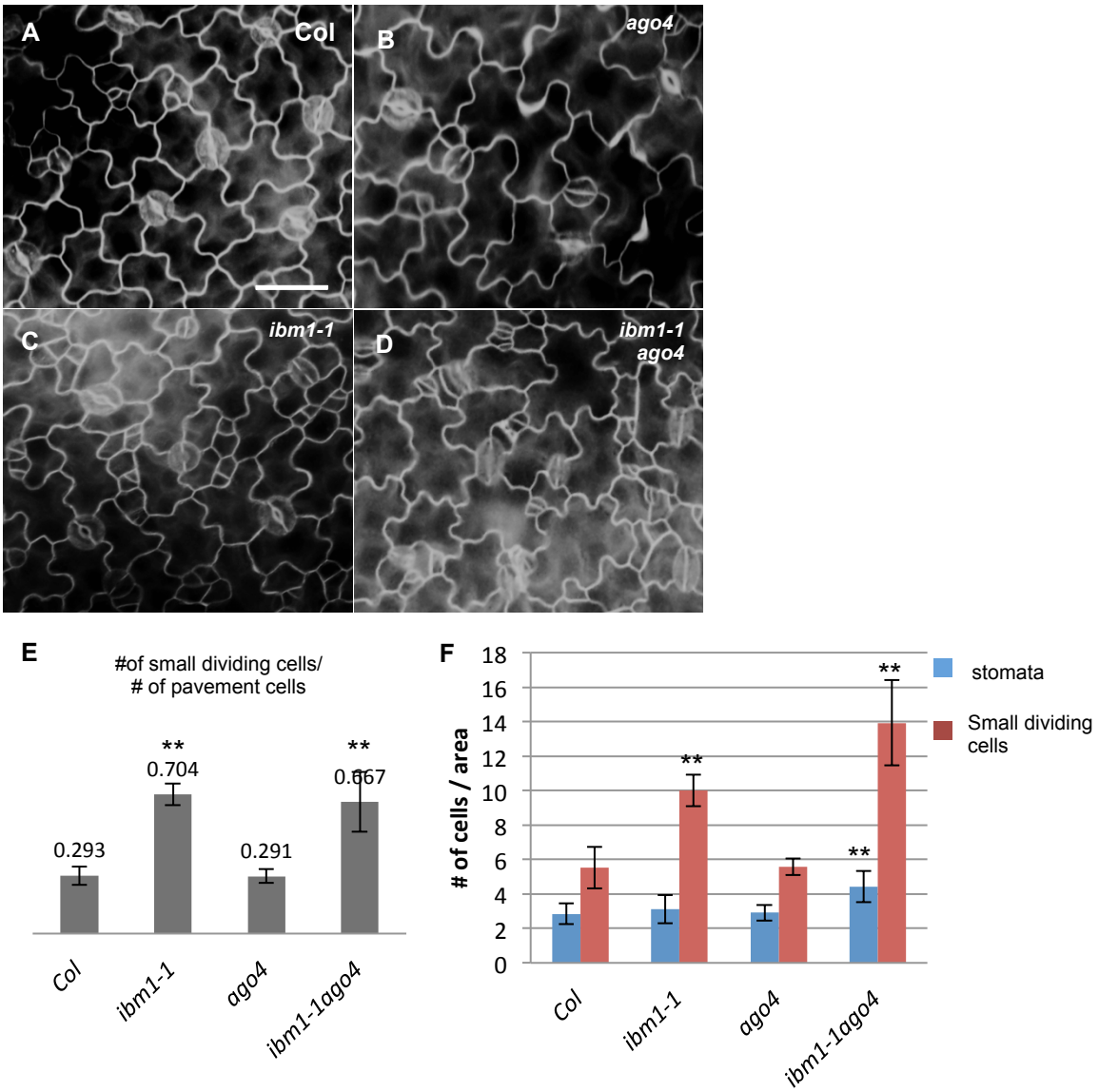

Fig. S9. *ibm1-1* is epistatic to *ago4* in stomatal development.
(A-D) Epi-fluorescent microscope images show 3-dpg adaxial codyledons of Col (A), *ago4* (B), *ibm1-1* (C) and *ibm1-1 ago4* (D). The *ibm1-1 ago4* double mutant resembled *ibm1-1*. Cell outlines were marked by FM1-43 staining. Scale bars in (A) = 30 μm. Others (B-D) are at the same scale.
(E) Histogram shows the ratio of the total number of small dividing cells relative to that of the pavement cells in different genotypes. Significant differences, * $P < 0.05$, ** $P < 0.01$; one-way ANOVA with Bonferroni multiple comparison (n = 6; ± SD).
(F) Quantification of the number of stomata and small dividing cells collected from same sized areas. Values in (E-F) are means ± SD. Significant differences * $P < 0.05$, ** $P < 0.01$; Student's *t*-test with Bonferroni Correction was used to compare the mutant values to those of Col.

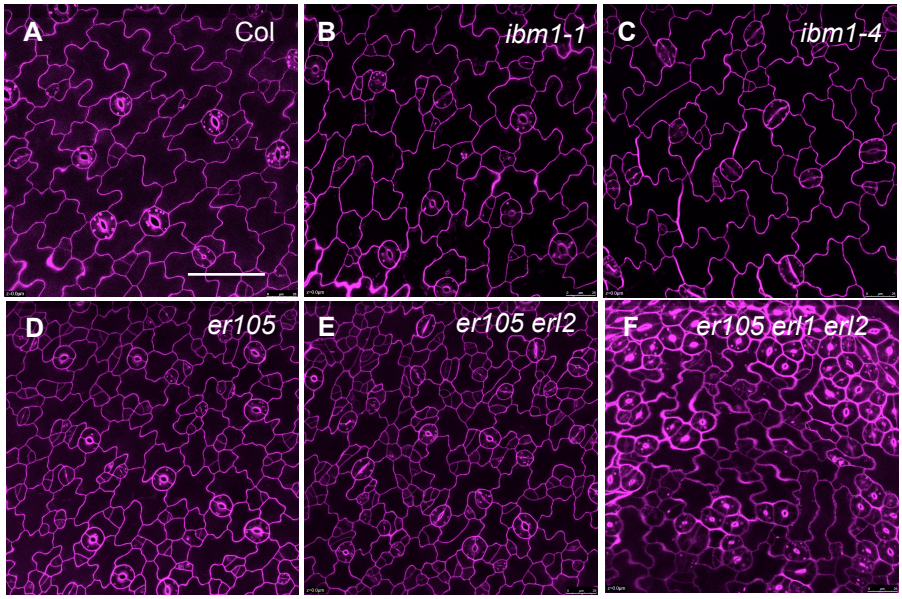

Fig. S10. Phenotype comparison of *ibm1* and *er* mutants.
(A-F) Confocal images show 3-dpg adaxial cotyledons of Col (A), *ibm1-1* (B), *ibm1-4 (C), er105* (D), *er105 erl2* (E), *er105 erl1 erl2 (F)* and *ibm1-1 er105. ibm* mutants show milder phenotype than *er105* loss-of-function plants. Cell outlines were marked by propidium iodide staining (magenta). Scale bars in (A) = 25 μm. Others (B-H) are at the same scale.

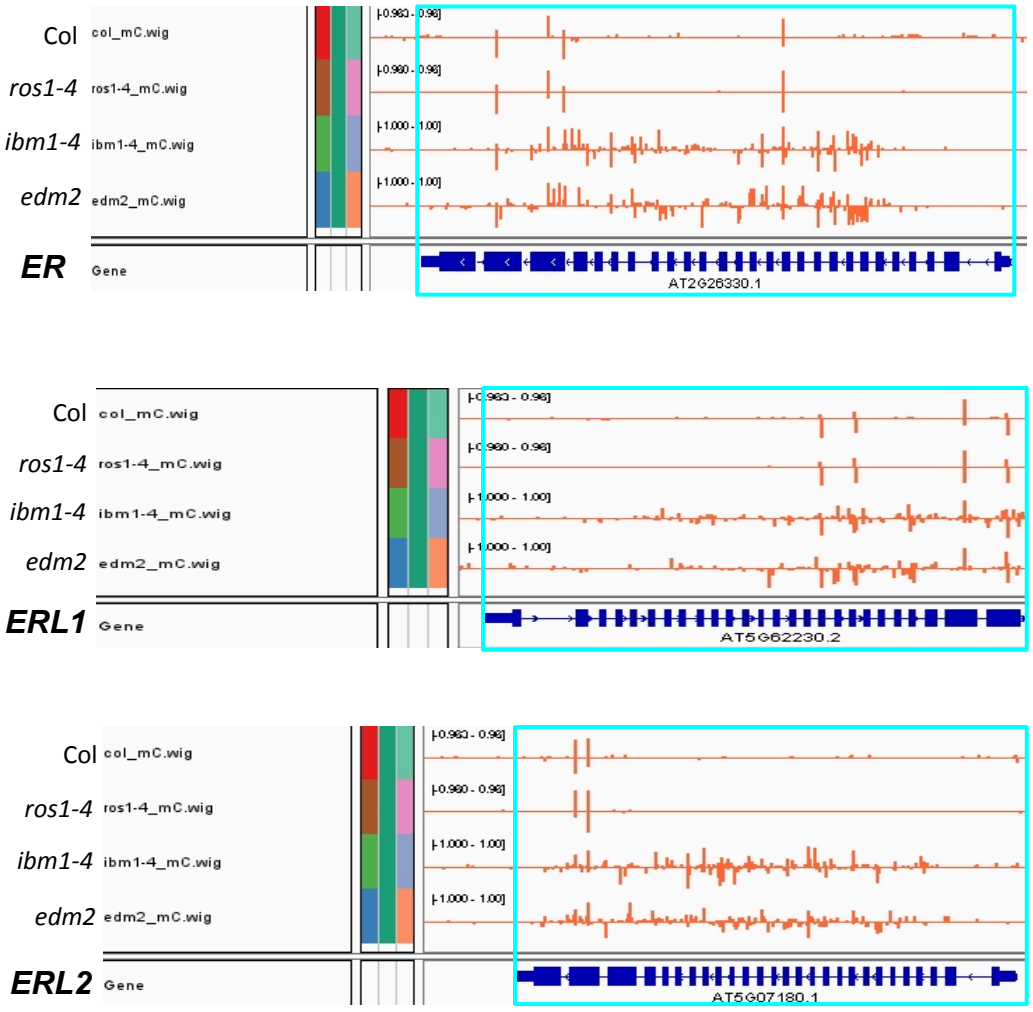

Fig. S11. *ER* genes are hypermethylated in *ibm1* and *edm2* mutants, but not in *ros1* mutants.
Integrated genome viewer shows the whole genome bisulfite sequencing of *ER* gene (top), *ERL1* (middle) and *ERL2* (bottom) in the wild-type (Col), *ros1-4*, *ibm1-4*, and *edm2-4* mutants. Orange bars indicate the sites of cytosine methylation.

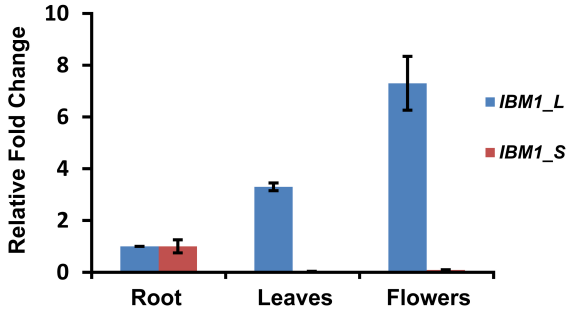

Fig. S12. Expression levels of *IBM1-L and IBM1-S* in different plant tissues.

Relative expression levels of *IBM1* variants (*IBM1-L* and *IBM1-S)* in different tissues were normalized to the transcription level in roots. Data were collected from three replicates. Errors bars indicate ± SD.

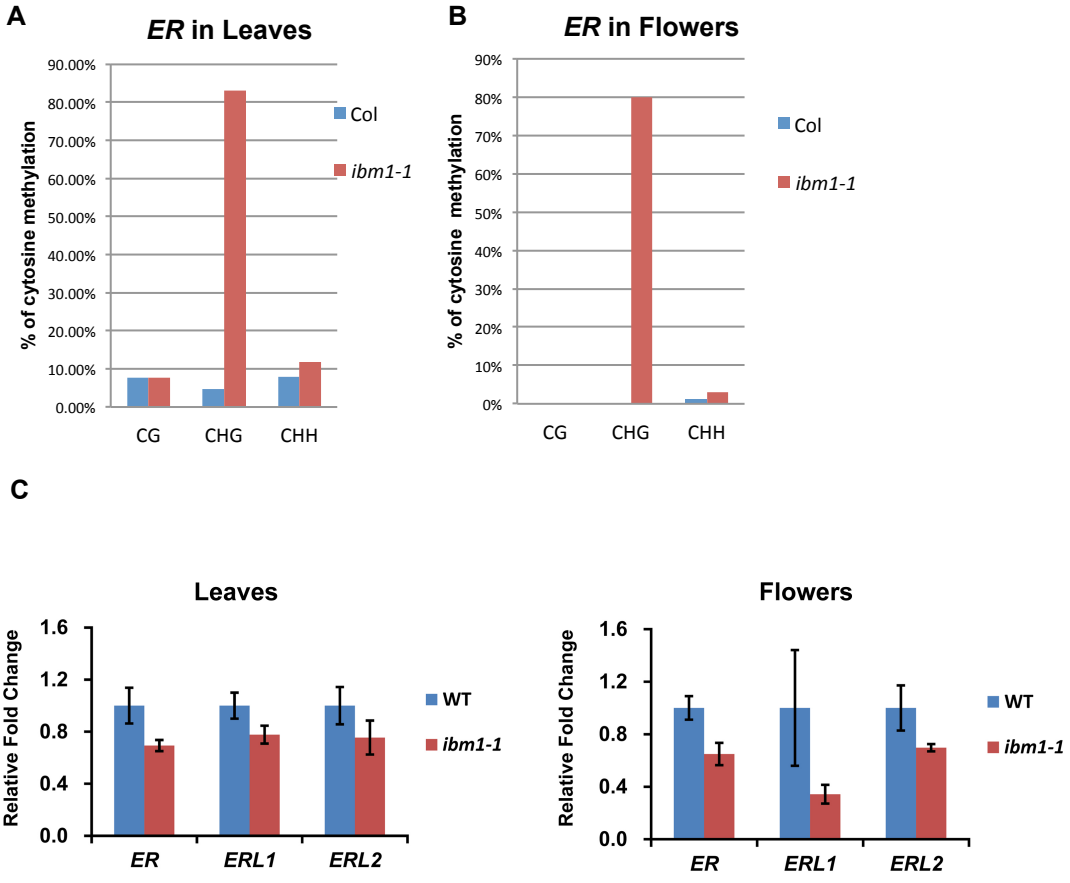

Fig. S13. Methylation and expression levels of *ER* gene in leaves and flowers.

(A-B) Individual bisulfite sequencing analyses of CG, CHG, CHH methylation sites in *ER* in leaves (A) or in flowers (B). At least 10 clones were selected from each sample.

(C) Real-time PCR analyses of *ER*, *ERL1* and *ERL2* expression in different tissues of Col and *ibm1* mutants. Data were collected from three replicates and the expression fold changes were normalized to the transcription level in Col. Errors bars indicate ± SD.

Supplemental Tables

	WT (CG)	*ibm1-4* (CG)	fold change	WT (CHG)	*ibm1-4* (CHG)	fold change	WT (CHH)	*ibm1-4* (CHH)	fold change
ER	0.375818119	0.416845111	**1.109167147**	0.008244168	0.327406049	**39.71365564**	0.02981933	0.087992667	**2.950859962**
ERL1	0.2919574	0.306628711	**1.050251547**	0.010012084	0.277957569	**27.76220905**	0.037113758	0.158935635	**4.282391317**
ERL2	0.298761062	0.318145484	**1.064882692**	0.003967043	0.312062646	**78.66379215**	0.018156851	0.12095968	**6.66193053**
TMM	0.007407407	0.004251701	**0.573979667**	0.00949094	0.004665112	**0.491533188**	0.028185217	0.009663446	**0.342855122**
SERK1	0.366955728	0.36997992	**1.008241299**	0.010269953	0.322149837	**31.36818986**	0.009121818	0.01997897	**2.190239939**
SERK2	0.501994302	0.475967957	**0.948154103**	0.010052657	0.36410403	**36.21968181**	0.013546989	0.015141087	**1.117671812**
BAK1/SERK3	0.406844106	0.416154936	**1.022885497**	0.013236267	0.357675112	**27.02235469**	0.019143118	0.011691824	**0.610758639**
SERK4	0.324214203	0.31440526	**0.969745488**	0.01099537	0.140983607	**12.82208801**	0.008513425	0.009006085	**1.057868622**
SPCH	0.042986425	0.041116006	**0.956488147**	0.011270492	0.000965251	**0.085644087**	0.057377049	0.014478764	**0.252344173**
MUTE	0.006916996	0.003015075	**0.435893703**	0.00433526	0.009419152	**2.172684453**	0.062138728	0.025117739	**0.40422036**
FAMA	0.014114326	0.005511811	**0.39051181**	0.008792966	0.003007519	**0.342036919**	0.059952038	0.020300752	**0.338616545**
EPF2	0.006097561	0.002645503	**0.43386249**	0.001805054	0.013303769	**7.370288645**	0.02166065	0.011086475	**0.511825592**
EPF1	0.009756098	0.002610966	**0.267624003**	0	0.01344086	**-**	0.018779343	0.029569892	**1.574596726**
SCRM2	0.007497657	0.003422704	**0.456503145**	0.006933501	0.001767565	**0.254931095**	0.024582414	0.011047282	**0.449397769**
MKK7	0.003038488	0.001812415	**0.596485818**	0.002245929	0.002245509	**0.999812995**	0.012352611	0.011976048	**0.969515514**
MKK4	0.029398859	0.032004197	**1.088620378**	0.003309067	0.004524887	**1.367420787**	0.015221707	0.009803922	**0.64407507**
MKK9	0.005199781	0.003685957	**0.708867739**	0.006282723	0.003573981	**0.568858598**	0.019371728	0.008577555	**0.442787293**
FLP	0.073458841	0.078310783	**1.066049803**	0.014193548	0.009972801	**0.702629181**	0.064946237	0.013145966	**0.202413051**
MYB88	0.004965243	0.028368794	**5.713475453**	0.003954974	0.166484517	**42.09497129**	0.022817159	0.026958106	**1.1814839**

MPK6	0.14977201	0.213101496	**1.422839261**	0.008166043	0.03891366	**4.765301873**	0.034025179	0.018646129	**0.548009725**
MKK5	0.007759457	0.004402516	**0.567374238**	0.006134969	0.001740644	**0.283724987**	0.032038173	0.013925152	**0.434642512**
MPK3	0.028571429	0.028009535	**0.98033371**	0.003225806	0.030090684	**9.328113346**	0.008870968	0.013190437	**1.486921946**
Stomagen	0.01754386	0	**0**	0.011363636	0.003610108	**0.317689514**	0.003787879	0.014440433	**3.812274099**

Table S1.Genomic methylation level of the genes that function in *Arabidopsis*stomatal development.

Red, > 25 times of fold change; Magenta, > 2-10 times of fold change.

qRT Actin2-F	GACCAGCTCTTCCATCGAGAA
qRT Actin2-R	CAAACGAGGGCTGGAACAAG
qRT-IBM1-F	TGTTACTAAGCTCCACTGCG
qRT-IBM1-SR	GGTTCTGAAATCATTATAGATGTGC
qRT-IBM1-L	CTCCATCATTTCCTCCTTGTTAGC
ERL2-RT-F	AGGCTGTGGATAACGAGGCC
ERL2-RT-R	GTGGAGACGGGACAAGTGAG
ERL1-RT-F	TAGGCACAGAAACATAGTCAG
ERL1-RT-R	TCTTAGCAATCCCGAAATCAG
ER-RT-F	TGAATGTGGCCAACAATGATCTGG
ER-RT-R	TTTTGAAATGCTCGGGGTATAGTGC
IBM1-4-23F	GCTGCTACCACTAGTTGCCAG
IBM1-4-24R	ACTGCCACGATAATGAGGTTG
LBb1.3	ATTTTGCCGATTTCGGAAC
ERg105	AAGAAGTCATTCAAAGATGTGA
ER105	AGCTGACTATACCCGATACTGA
ERg105RV	CTGCAATTGAAATTACACATG
SERK1-qF	CTACGCTAGTGAATCCTTGCACATG
SERK1-qR	GATTACTAGGAATCGGGCCAGTTATG
SERK2-qF	GCTGGGATCCTACGCTTGTTAATC
SERK2-qR	CAGATTCCCAAGATCGCTTGGAAC
SERK3-qF	GTCTTTGGGTATGGAGTCATGCTTC

SERK3-qR	GATTAGCTGCTCCACTTCTTCGTC
SERK4-qF	GTACTCCAAAGCTGGGATGCTAC
SERK4-qR	CAAGCTCCTCAGGTATCTCCCCTG

Table S2. Primers used in this study.